doi:10.1093/brain/awv077 BRAIN 2015: 138; 1548–1567 | 1548

BRAIN
A JOURNAL OF NEUROLOGY

Astrocytic TYMP and VEGFA drive blood–brain barrier opening in inflammatory central nervous system lesions

Candice Chapouly,[1,2,3,*] Azeb Tadesse Argaw,[1,2,3,*] Sam Horng,[1,2,3] Kamilah Castro,[1,2,3] Jingya Zhang,[1,2,3] Linnea Asp,[1,2,3] Hannah Loo,[1,2,3] Benjamin M. Laitman,[1,2,3] John N. Mariani,[1,2,3] Rebecca Straus Farber,[1,2,3] Elena Zaslavsky,[2,3,4] German Nudelman,[2,3,4] Cedric S. Raine[5] and Gareth R. John[1,2,3]

*These authors contributed equally to this work.

In inflammatory central nervous system conditions such as multiple sclerosis, breakdown of the blood–brain barrier is a key event in lesion pathogenesis, predisposing to oedema, excitotoxicity, and ingress of plasma proteins and inflammatory cells. Recently, we showed that reactive astrocytes drive blood–brain barrier opening, via production of vascular endothelial growth factor A (VEGFA). Here, we now identify thymidine phosphorylase (TYMP; previously known as endothelial cell growth factor 1, ECGF1) as a second key astrocyte-derived permeability factor, which interacts with VEGFA to induce blood–brain barrier disruption. The two are co-induced NFκB1-dependently in human astrocytes by the cytokine interleukin 1 beta (IL1B), and inactivation of *Vegfa in vivo* potentiates TYMP induction. In human central nervous system microvascular endothelial cells, VEGFA and the TYMP product 2-deoxy-D-ribose cooperatively repress tight junction proteins, driving permeability. Notably, this response represents part of a wider pattern of endothelial plasticity: 2-deoxy-D-ribose and VEGFA produce transcriptional programs encompassing angiogenic and permeability genes, and together regulate a third unique cohort. Functionally, each promotes proliferation and viability, and they cooperatively drive motility and angiogenesis. Importantly, introduction of either into mouse cortex promotes blood–brain barrier breakdown, and together they induce severe barrier disruption. In the multiple sclerosis model experimental autoimmune encephalitis, TYMP and VEGFA co-localize to reactive astrocytes, and correlate with blood–brain barrier permeability. Critically, blockade of either reduces neurologic deficit, blood–brain barrier disruption and pathology, and inhibiting both in combination enhances tissue preservation. Suggesting importance in human disease, TYMP and VEGFA both localize to reactive astrocytes in multiple sclerosis lesion samples. Collectively, these data identify TYMP as an astrocyte-derived permeability factor, and suggest TYMP and VEGFA together promote blood–brain barrier breakdown.

1 Corinne Goldsmith Dickinson Centre for MS, Icahn School of Medicine at Mount Sinai, New York, NY 10029 USA
2 Friedman Brain Institute, Icahn School of Medicine at Mount Sinai, New York, NY 10029 USA
3 Department of Neurology, Icahn School of Medicine at Mount Sinai, New York, NY 10029 USA
4 Department of Systems Biology, Icahn School of Medicine at Mount Sinai, New York, NY 10029 USA
5 Department of Pathology (Neuropathology), Albert Einstein College of Medicine, Bronx, NY 10461, USA

Correspondence to: Gareth R. John,
Corinne Goldsmith Dickinson Centre for Multiple Sclerosis,
Icahn School of Medicine at Mount Sinai,
New York,
NY 10029 USA
E-mail: gareth.john@mssm.edu

Received October 17, 2014. Revised January 16, 2015. Accepted January 26, 2015. Advance Access publication March 24, 2015

Keywords: blood–brain barrier; endothelium; tight junction; astrocyte; endothelial cell growth factor

Abbreviations: 2DLR = 2-deoxy-L-ribose; CMVEC = central nervous system microvascular endothelial cell; DDR = 2-deoxy-D-ribose; EAE = experimental autoimmune encephalitis

Introduction

The blood–brain barrier acts as a selective interface separating the CNS from the periphery (Zlokovic, 2008). It exists at the level of CNS microvascular endothelial cells (CMVECs), which use tight junctions to seal the paracellular space, allowing transporters and channels to control transendothelial trafficking (Hawkins and Davis, 2005). Endothelial tight junctions rely for their integrity on transmembrane proteins, notably claudin 5 (CLDN5) and occludin (OCLN), and the blood–brain barrier fails to seal in *Cldn5*$^{-/-}$ mice (Saitou *et al.*, 1998; Nitta *et al.*, 2003; Wolburg *et al.*, 2003). Endothelial barrier formation and maintenance are controlled by astrocytes and pericytes (Bogler and Noble, 1994; Hayashi *et al.*, 1997; Bush *et al.*, 1999; Armulik *et al.*, 2010; Bell *et al.*, 2010; Daneman *et al.*, 2010), and these are also implicated in blood–brain barrier disruption in disease (Argaw *et al.*, 2009; Bell *et al.*, 2010).

Blood–brain barrier breakdown is a widespread, early and prominent feature of lesion pathogenesis in inflammatory CNS conditions including multiple sclerosis (Bruck *et al.*, 1997), neuromyelitis optica and viral encephalitis (Dallasta *et al.*, 1999), and in hypoxic/ischaemic syndromes and traumatic injury (Sandoval and Witt, 2008). In inflammatory disorders, blood–brain barrier permeability correlates with clinical exacerbation and lesion activity (Bruck *et al.*, 1997) and with the presence of irreversible neuropathology (Miller *et al.*, 1998). Blood–brain barrier opening results in oedema, disruption of metabolic function, excitotoxicity, and parenchymal entry of autoantibodies and plasma proteins that potentiate inflammation and limit repair (Schluesener *et al.*, 1987; Adams *et al.*, 2007; Germano *et al.*, 2007; Schachtrup *et al.*, 2007). Blood–brain barrier disruption also facilitates ingress into the CNS parenchyma of T and B lymphocytes, monocyte-derived macrophages, and polymorphonuclear leucocytes (Graesser *et al.*, 2002; Gorina *et al.*, 2014). In conditions such as multiple sclerosis, therapies for clinical exacerbation are limited. Targeting blood–brain barrier disruption may effectively limit tissue damage and relapse severity (DeAngelis and Lublin, 2008).

Recently, we identified a key pathway linking reactive astrocytes to blood–brain barrier breakdown (Argaw *et al.*, 2006, 2009, 2012). Transcriptional profiling revealed that reactive astrocytes express vascular endothelial growth factor A (VEGFA) (Argaw *et al.*, 2006), an important driver of angiogenesis also implicated in permeability syndromes (Collins *et al.*, 1993; Yeo *et al.*, 1993; Carmeliet *et al.*, 1996; Ferrara *et al.*, 1996; Dobrogowska *et al.*, 1998; Proescholdt *et al.*, 2002). Using mice with conditional inactivation, we confirmed astrocyte-derived VEGFA as an important inducer of blood–brain barrier disruption, acting in part via endothelial nitric oxide synthase (NOS3)-mediated downregulation of endothelial CLDN5 and OCLN (Argaw *et al.*, 2009, 2012). Critically, genetic or therapeutic targeting of *Vegfa* or *Nos3* restricted pathology and clinical deficit in the multiple sclerosis model, experimental autoimmune encephalomyelitis (EAE) (Argaw *et al.*, 2012).

Interestingly, despite these advances, our studies *in vivo* reveal that blockade of VEGFA signalling does not completely abrogate blood–brain barrier disruption and lesion formation in inflammatory models, suggesting contributions of additional pathways. Here, we now report an expanded transcriptional screen of a primary model of human reactive astrogliosis, which reveals co-expression of a second critical inducer of endothelial plasticity and remodelling, thymidine phosphorylase (TYMP; previously known as endothelial cell growth factor-1, ECGF1). Like VEGFA, TYMP is heavily implicated in tumour angiogenesis, in conditions including ductal breast carcinoma (Engels *et al.*, 1997), colon carcinoma (Saeki *et al.*, 1997), gastric carcinoma (Maeda *et al.*, 1996), pancreatic carcinoma (Takao *et al.*, 1998), oesophageal carcinoma (Igarashi *et al.*, 1998), non-small-cell lung cancer (Koukourakis *et al.*, 1997), and Paget's disease (Ellis *et al.*, 2002). In some tumours, VEGFA is strongly expressed and linked with increased microvascular density and poor prognosis (Takanami *et al.*, 1997; Uchida *et al.*, 1998). In others, sometimes of the same classification, TYMP fulfils the same function with a similarly poor outlook (Ellis *et al.*, 2002). In still others, both are expressed and microvascular density further increased (Toi *et al.*, 1995; Tsujitani *et al.*, 2004). TYMP/ECGF1 was first described as a platelet-derived angiogenic activity (Ishikawa *et al.*, 1989), and is now known to correspond to the enzyme thymidine phosphorylase (Furukawa *et al.*, 1992). Its effects depend on catalysis of thymidine to thymine plus 2-deoxy-D-ribose (DDR), with DDR the active driver of endothelial responses (Moghaddam *et al.*, 1995).

We now demonstrate roles for both pathways in blood–brain barrier permeability in inflammatory CNS disease. Our data show that TYMP and VEGFA are co-induced in human astrocytes by the cytokine interleukin 1 beta (IL1B), an important driver of inflammatory lesion pathogenesis (Herx and Yong, 2001), acting via the transcription factor NFκB1. Suggesting that expression of the two is interlinked, inactivation of *Vegfa* potentiates TYMP induction *in vivo*. Importantly, in human CMVEC cultures, VEGFA and DDR each downregulate CLDN5 and OCLN and drive permeability, and together they produce

stronger effects. Transcriptional profiling of human CMVEC cultures reveals that these outcomes represent part of a wider program of endothelial plasticity. DDR and VEGFA each induce distinct endothelial transcriptional patterns associated with permeability, motility, remodelling and angiogenesis, and together regulate a third unique transcriptional cohort. Functionally, each promotes viability and proliferation, and together they cooperatively drive endothelial motility and angiogenesis. Introduction of either into mouse cortex induces blood–brain barrier breakdown, and together they produce severe barrier disruption. In IL1B-induced inflammatory lesions in mice, and in EAE, TYMP and VEGFA co-localize to reactive astrocytes, and their expression correlates with endothelial tight junctions disruption and blood–brain barrier breakdown. Critically, blockade of either in EAE restricts blood–brain barrier disruption, paralysis and tissue damage, and blocking both in combination enhances tissue preservation. Suggesting significance in human disease, both localize to reactive astrocytes in lesion samples from patients with multiple sclerosis.

Collectively, this work identifies TYMP as an important astrocyte-derived permeability factor in inflammatory CNS disease, and suggests that it interacts with VEGFA to promote blood–brain barrier breakdown.

Materials and methods

Additional technical details are available in the online Supplementary material.

Cytokines and growth factors

Human IL1B, IL17 and CSF2 (previously known as GM-CSF), and mouse $VEGFA_{165}$ were purchased from Peprotech. Human IFNG, IL6, TNF, TGFB1 and VEGFA were from R&D Systems. Based on previous studies, human VEGFA was routinely used at 100 ng/ml, whereas other factors were used at 10 ng/ml (Argaw *et al.*, 2006). Mouse $VEGF_{165}$ was used at 20 ng/µl (Argaw *et al.*, 2006).

Drugs

DDR and its inhibitor 2-deoxy-L-ribose (2DLR) were purchased from Sigma-Aldrich and used at 1–10 µM (130–1300 ng/ml). Anti-VEGFR2 blocking antibody and control IgG (1000 ng/ml) were from R&D Systems. JAK inhibitor 1 (CAS 457081-03-7) was from EMD Millipore and used at 15 mM, compatible with its known IC_{50}.

Cell culture

Primary human foetal astrocyte cultures were established from three different brains as described (Lee *et al.*, 1992). Primary human or bovine CMVEC were purchased from Cell Systems Inc. and cultured in complete serum containing medium. All studies were approved by the appropriate Institutional Review Board.

Adenoviral transfer *in vitro*

Astrocytes in 100 mm culture dishes were infected with adenovirus encoding a proteolysis-resistant (S32,36E) super-repressor form of (Ad-IκBα) or adenovirus containing the CMV promoter, but not IκBα (Ad-Ctrl), at a concentration of 104 viral particles per cell (Argaw *et al.*, 2006). Infection was left to proceed for 24 h, then cultures washed and treated as described.

Microarray analysis

Primary human astrocytes or CMVEC were treated as described, and total RNA extracted at times shown using the RNeasy® Mini kit (Qiagen). RNA quality was assessed using a NanoDrop™ spectrophotometer. Total RNA was converted to cDNA and subsequently into biotin-labelled cRNA using a commercially available kit (Illumina) according to the manufacturer's instructions, and 1.5 µg of cRNA hybridized to Illumina HumanHT-12 v4 Expression Beadchips. Raw expression data were subjected to quantile normalization and low-intensity value filtering using a cut-off of 200, then were log2 transformed (MatLab, MathWorks). Differentially expressed genes between the control and experimental groups were identified using unpaired two-tailed *t*-test with false discovery rate (FDR) correction, as having a corrected *P*-value <0.05 and additionally filtered a standard ratiometric induction/repression cut-off as described in the text. Qualifying genes in studies using astrocytes were subjected to hierarchical clustering using Cluster© 3.0 software (Michael Eisen, UC Berkeley), and converted to a colorimetric format using Java Treeview (Alok Saldanha, Open Source Clustering Software). Analysis to identify physiologic or disease functions most relevant to differentially expressed gene cohorts was carried out using Ingenuity© software (Ingenuity Systems), which uses Fisher's exact test to calculate a *P*-value that association between each biological function and the cohort is due to chance alone.

Mice

mGfapCre mice were made in the laboratory of Dr Michael Sofroniew (UCLA) (Garcia *et al.*, 2004). Cre expression is astrocyte-specific except in areas of adult neurogenesis, where it is also observed in some neural progenitors (Garcia *et al.*, 2004). $Vegfa^{fl}$ mice were made by Dr Napoleone Ferrara (UCSD) and have been reported (Gerber *et al.*, 1999). $GfapCre{:}Vegfa^{+/fl}$ mice were crossed with $Vegfa^{fl/fl}$ animals to generate $GfapCre{:}Vegfa^{fl/fl}$ mice and controls. Genotyping primers were: *GfapCre* forward (GfF) ACCAGCCAGCTA TCAACTC, reverse (GfR) TATACGCGTGCTAGCGAAGAT CTCCATCTT CCAGCAG, band 350 bp. $Vegfa^{fl}$ forward (VfF) CCTGGCCCTCAAGTACACCTT, reverse (VfR) TCCGTACGACGCATTTCTAG, band 108 bp (wild-type) 148 bp (flox). PCR conditions were 94°C 4 min then 35 cycles 94°C 30 s, 56°C 30 s, 72°C 30 s, then 72°C 10 min. C57BL/6 mice were from Jackson.

Statistical analyses

For multiple comparisons, one-way ANOVA followed by Bonferroni post-test was used. Student's *t*-test was used to compare two groups of matched samples. Spearman rank

correlation coefficient was used to test for correlation of two variables. In transcriptional profiling studies, differentially expressed genes between the control and experimental groups were identified using unpaired two-tailed *t*-test with FDR correction. In all cases, $P < 0.05$ was considered significant.

Results

IL1B co-induces TYMP and VEGFA in primary human astrocyte cultures

Transcriptional profiling of a human model of reactive astrogliosis using a larger-scale platform than we have previously reported (Argaw *et al.*, 2006) revealed a wide cohort of transcripts linked to endothelial plasticity and remodelling (Fig. 1). Human astrocyte cultures prepared from three different brains and screened with molecular markers to ensure culture purity were treated with IL1B (10 ng/ml), a key driver of inflammatory lesion pathogenesis and reactive astrogliosis (Lee *et al.*, 1992; Herx and Yong, 2001) (Supplementary Fig. 1A). Resulting transcriptional patterns were compared with vehicle controls using 47 300 element human Illumina Beadarrays© (Fig. 1A). Genes induced or repressed $>\log_2$ 2-fold and significant using Student's *t*-test with FDR correction $P < 0.05$ were subjected to bioinformatics analysis and validation.

Importantly, this approach identified multiple transcripts implicated in angiogenesis and/or endothelial remodelling, notably including *TYMP*, the vascular endothelial growth factors *VEGFA* and *VEGFC*, and the VEGF co-receptor *NRP1* (Ishikawa *et al.*, 1989; Leung *et al.*, 1989; Jeltsch *et al.*, 1997; Soker *et al.*, 1998). Also identified were the regulator of angiogenesis *ADAMTS1* (Vazquez *et al.*, 1999), and the inflammation-induced endothelial plasticity genes *NLF2* (now known as *C2CD4B*) and *IER3* (Warton *et al.*, 2004; Tang *et al.*, 2006) (Fig. 1A). Additionally, IL1B induced astrocytic expression of the matrix metalloproteinases *MMP3*, *MMP7*, *MMP9* and *MMP10*, linked to blood–brain barrier breakdown and leucocyte entry into the CNS (Bar-Or *et al.*, 2003). Compatible with previous reports (Hurwitz *et al.*, 1992), IL1B-treated astrocytes also expressed the adhesion molecules *VCAM1*, *ICAM1* and E-selectin (*SELE*) (Lyck and Engelhardt, 2012). Further suggesting that reactive astrogliosis regulates inflammatory cell infiltration into and within CNS lesions, IL1B robustly induced multiple CXC and CC chemokines, including *CXCL1*, *CXCL2*, *CXCL5*, *CXCL6*, *CXCL10*, *CXCL12* and *CXCL14*, and *CCL5*, *CCL8* and *CCL20* (Ransohoff *et al.*, 1996) (Fig.1A). Inference of function calculated via Ingenuity© gene ontology (GO) analysis identified immunologic disease, inflammatory disease and tissue-specific inflammation as outcomes most significantly associated with this program (Fig. 1B).

Co-induction of TYMP and VEGFA was a particularly compelling finding within this data set. Importantly, both are widely implicated in tumour angiogenesis, functioning in complementary or collaborative roles (Toi *et al.*, 1995; Engels *et al.*, 1997; Takanami *et al.*, 1997; Uchida *et al.*, 1998; Ellis *et al.*, 2002; Tsujitani *et al.*, 2004). Their co-induction in reactive astrocytes suggested similar interactions in driving endothelial remodelling and permeability in inflammatory CNS lesions.

Protein-level studies validated IL1B induction of TYMP and VEGFA in human astrocyte cultures (Fig. 1C and D); these responses were dose-dependent (data not shown). Further suggesting co-regulation of the two genes, interferon gamma (IFNG), a cytokine also expressed in inflammatory lesions, potentiated IL1B-mediated induction of both (Fig. 1C and D). Similar to VEGFA (Argaw *et al.*, 2006), confocal imaging confirmed induction of TYMP immunoreactivity in IL1B-treated cultures, and robust immunoreactivity in astrocytes exposed to IL1B + IFNG together (Fig. 1E). Confirming cell type specificity, and again similar to VEGFA (Argaw *et al.*, 2006, 2012), TYMP was sensitive to IL1B in astrocytes but no induction occurred in CMVEC (Fig. 1F), nor was expression observed in either cell type in response to other cytokines or growth factors, including VEGFA, CSF2, IL17 (Fig. 1F and G), TNF, IL6, or TGFB1 (data not shown). Notably, the time courses of TYMP and VEGFA induction in astrocytes were also identical: for both genes induction in response to 10 ng/ml IL1B was first detectable at the protein level at 12–24 h post-treatment, reached a plateau at 48 h, and persisted until at least 72 h (Fig. 1H and I).

Co-induction of TYMP and VEGFA in primary human astrocytes is NFκB1-dependent

Further analyses revealed that IL1B uses the same mechanism to induce both TYMP and VEGFA in primary human astrocytes. IL1B activates the transcription factors NFκB1 and AP-1, with nuclear translocation of the former resulting from degradation of IκBα (Vallabhapurapu and Karin, 2009), and of the latter via phosphorylation of p38 and JNK/SAPK MAP kinases (John *et al.*, 2001). We used an adenovirus expressing a proteolysis-resistant (S32,36E) IκBα super-repressor to inhibit NFκB1 (Kim *et al.*, 2004), and siRNA for *p38* to inhibit AP-1 activity. Induction of both TYMP and VEGFA was abolished in cultures infected with the viral super-repressor (Fig. 1J and K), whereas silencing of *p38* had no effect (data not shown). Interestingly, we have also previously identified a potential role for the bHLH transcription factor HIF1A in IL1B-mediated VEGFA induction, and HIF1A is itself NFκB1-sensitive in human cultures (Argaw *et al.*, 2006). Further demonstrating specific involvement of NFκB1, blockade of other pathways not activated by IL1B, for example using inhibitors of JAK-STAT signalling, did not prevent TYMP induction (Supplementary Fig. 1B).

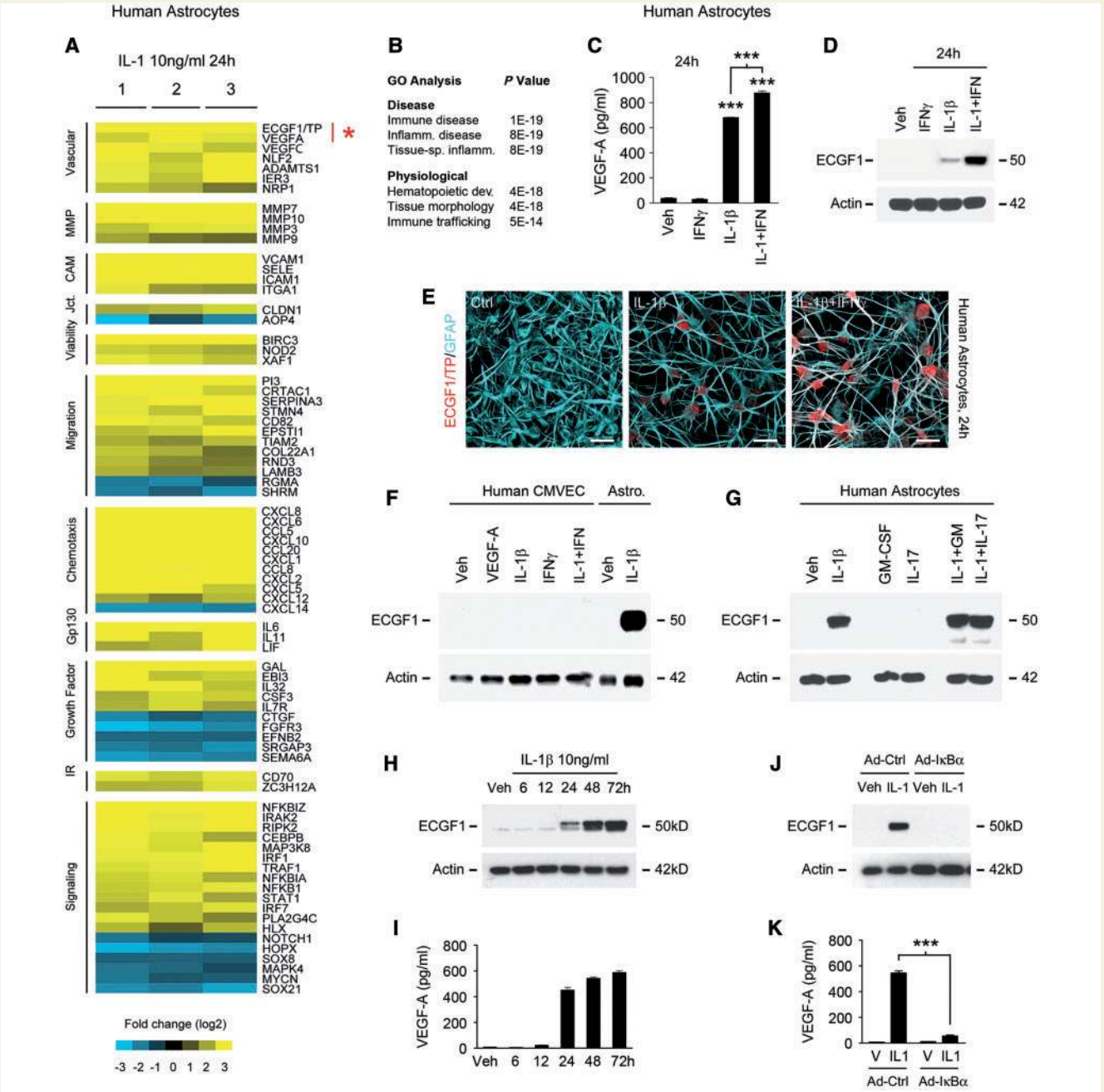

Figure 1 In primary human astrocytes, IL1B induces expression of TYMP, a novel candidate driver of blood–brain barrier disruption. (**A**) Results of Illumina HumanHT-12 v4 Beadchip© transcriptional profiling of primary human astrocytes treated with IL1B 10 ng/ml for 24 h. Data for three separate cultures screened for purity (as detailed in Supplementary Fig. 1A) are shown, subjected to log2 transformation and colour-coded according to the scale presented below, filtered using Student's *t*-test and FDR correction $P < 0.05$ and sorted using Cluster/Treeview software. TYMP (ECGF1) is among the most strongly induced transcripts (mean FC 10.52) in astrocytes exposed to IL1B, comparable in magnitude to that of the blood–brain barrier permeability factor VEGFA. Other molecules downstream of IL1B include upregulation of matrix metalloproteinases, CXC/CC chemokines, and adhesion molecules, all implicated in blood–brain barrier permeability. (**B**) GO analysis of data shown in **A** using Ingenuity© software reveals that functional pathways downstream of IL1B include immunologic and inflammatory disease, and immune cell trafficking. (**C** and **D**) Sandwich ELISA (**C**) and immunoblotting (**D**) demonstrate that VEGFA and TYMP are both induced by IL1B at 24 h and that induction is potentiated by IFNG, which in isolation is not sufficient for these effects. (**E**) Immunocytochemistry confirms that TYMP protein is induced in the cytoplasm of human astrocytes exposed to IL1B, and more strongly by IL1B + IFNG in combination. (**F** and **G**) Immunoblotting of human cultures demonstrates that TYMP induction by IL1B + IFNG is astrocyte-specific. (**F**) TYMP is not induced in CMVEC by these cytokines or 100 ng/ml VEGFA. (**G**) Astrocytic TYMP induction does not occur in response to other inflammatory cytokines such as CSF2 (GM-CSF) or IL17, nor is it potentiated by the addition of these factors to IL1B. (**H** and **I**) Both astrocytic TYMP and VEGFA induction in response to 10 ng/ml IL1B are first observed at 24 h and peak at 48 h, and persist at 72 h. (**J** and **K**) Blocking activity of the IL1B-activated transcription factor NFκB1 using an adenoviral IκBα super-repressor prevents induction of both TYMP and VEGFA in primary human astrocytes. See also Supplementary Fig. 1B. Results in all panels are representative of three independent experiments in separate cultures. Statistics: **A** = *t*-test plus FDR correction; **C** and **K** = ANOVA plus Bonferroni test. Scale bars in **E** = 10 μm.

Collectively, these results demonstrated NF-κB-dependent co-induction of TYMP and VEGFA in primary human astrocytes.

Astrocytic TYMP induction by IL1B *in vivo* is potentiated by conditional *Vegfa* inactivation

Studies in cancer have shown that VEGFA is expressed by and drives angiogenesis in some tumours, whereas TYMP fulfils the equivalent function in others (Takanami *et al.*, 1997; Uchida *et al.*, 1998; Ellis *et al.*, 2002). In still others, both act cooperatively (Toi *et al.*, 1995; Tsujitani *et al.*, 2004). To determine if expression of the two is interrelated, we tested whether inactivation of one impacts the other. We thus examined TYMP expression in a focal IL1-induced model of CNS inflammation in mice with astrocyte-specific *Vegfa* inactivation (*mGfapCre:Vegfa*$^{fl/fl}$), the blood–brain barrier phenotype of which we have described previously (Argaw *et al.*, 2012) (Fig. 2 and Supplementary Fig. 1).

Initially, we validated astrocyte-specific TYMP and VEGFA induction *in vivo* in controls in the IL1 model. We have previously shown that injection of the adenoviral vector AdIL-1 (10^7 pfu) into 12-week-old mouse cerebral cortex induces focal inflammation, reaching maximal activity at 7 days post-induction and characterized by GFAP$^+$ reactive astrogliosis, downregulation of endothelial CLDN5 and OCLN, and blood–brain barrier opening (Argaw *et al.*, 2009, 2012). In cortices from uninjected or empty vector-injected wild-type or *Vegfa*$^{fl/fl}$ controls or experimental *mGfapCre:Vegfa*$^{fl/fl}$ mice, we detected no expression of VEGFA or TYMP. However, both were strongly induced in AdIL-1 lesions at 7 days post-induction in wild-type or non-*Cre Vegfa*$^{fl/fl}$ controls, and localized specifically to reactive GFAP$^+$ astrocytes (Fig. 2A–E and Supplementary Fig. 1C–E). Moreover, and importantly, TYMP induction was strongly potentiated in astrocytes in lesions in *mGfapCre:Vegfa*$^{fl/fl}$ mice (Fig. 2B, F and Supplementary Fig. 1D).

Together, these studies demonstrated astrocyte-specific induction of both TYMP and VEGFA in inflammatory lesions in the CNS of adult mice. Moreover, astrocytic TYMP induction by IL1B *in vivo* was potentiated by conditional *Vegfa* inactivation, suggesting that expression of the two genes is interrelated in this context.

DDR and VEGFA downregulate endothelial tight junction proteins

We next examined the impact of DDR and VEGFA on human CMVEC, both in terms of patterns of gene regulation (Fig. 2G–M and Supplementary Tables 1–3), and their translation into effects on proliferation, viability, migration, angiogenesis and permeability (Figs 2N, O and 3A–F). VEGFA exerts its effects on CMVEC via activation of the receptor tyrosine kinase VEGFR2/KDR/Flk-1 (Olsson *et al.*, 2006). TYMP acts via production of DDR (Furukawa *et al.*, 1992; Moghaddam *et al.*, 1995), the downstream effectors of which are incompletely characterized, but this mechanism is known to activate transcription of target genes (Bijnsdorp *et al.*, 2011).

Downregulation of endothelial tight junction transmembrane proteins has been implicated as a key event in VEGF-induced blood–brain barrier opening (Argaw *et al.*, 2009). Thus, we compared effects of DDR and VEGFA on CLDN5 and OCLN expression in CMVEC cultures. These studies revealed that both CLDN5 and OCLN were strongly downregulated by physiologic concentrations of DDR (1 µM/130 ng/ml) as well as by VEGFA (100 ng/ml) (Fig. 2G and Supplementary Fig. 1F). Moreover, these effects were potentiated when both factors were used together (Fig.2G). Treatment with astrocyte IL1B conditioned medium also resulted in downregulation of CLDN5, and this decrease was blocked by αVEGFA receptor 2 (αVR2) and the competitive DDR inhibitor, 2DLR, further confirming that astrocyte-mediated downregulation of endothelial tight junctions proteins is effected via DDR and VEGFA (Fig 2H).

VEGFA and DDR elicit distinct transcriptional patterns linked to plasticity and permeability

For wider unbiased analysis of transcriptional patterns, we returned to the human Beadarray© platform (Fig. 2I–M and Supplementary Tables 1–3). Human CMVEC (three independent preparations) were screened for culture purity using molecular markers (Supplementary Fig. 1G), then treated with DDR, VEGFA, or both, and RNA harvested at 24 h. Preliminary studies indicated that VEGFA and DDR produce smaller transcriptional changes than proinflammatory cytokines such as IL1B, thus regulated transcripts were defined as having expression altered by $>\log_2$ 0.5-fold, and significant using *t*-test with FDR correction $P < 0.05$. Results are presented as a colour-coded schematic in Fig. 2I, and the 20 most strongly induced transcripts for each condition shown in Fig. 2J–L, similarly colour-coded. All regulated transcripts and their functions are in Supplementary Tables 1–3, and functions summarized in Fig. 2M.

Importantly, these studies revealed that DDR and VEGFA downregulation of endothelial tight junction proteins represents part of a more far-reaching transcriptional pattern. DDR and VEGFA induced distinct transcriptional programs, but each was indicative of endothelial plasticity, remodelling and/or angiogenesis. Moreover, exposure of human CMVEC to DDR and VEGFA together produced regulation of a third unique cohort also indicative of a remodelling program.

VEGFA regulated 80 genes in these studies, whereas the DDR-regulated profile was 41 genes (Fig. 2I–K and Supplementary Tables 1 and 2). Co-treatment produced a larger cohort of 119 genes (Fig. 2I, L and Supplementary

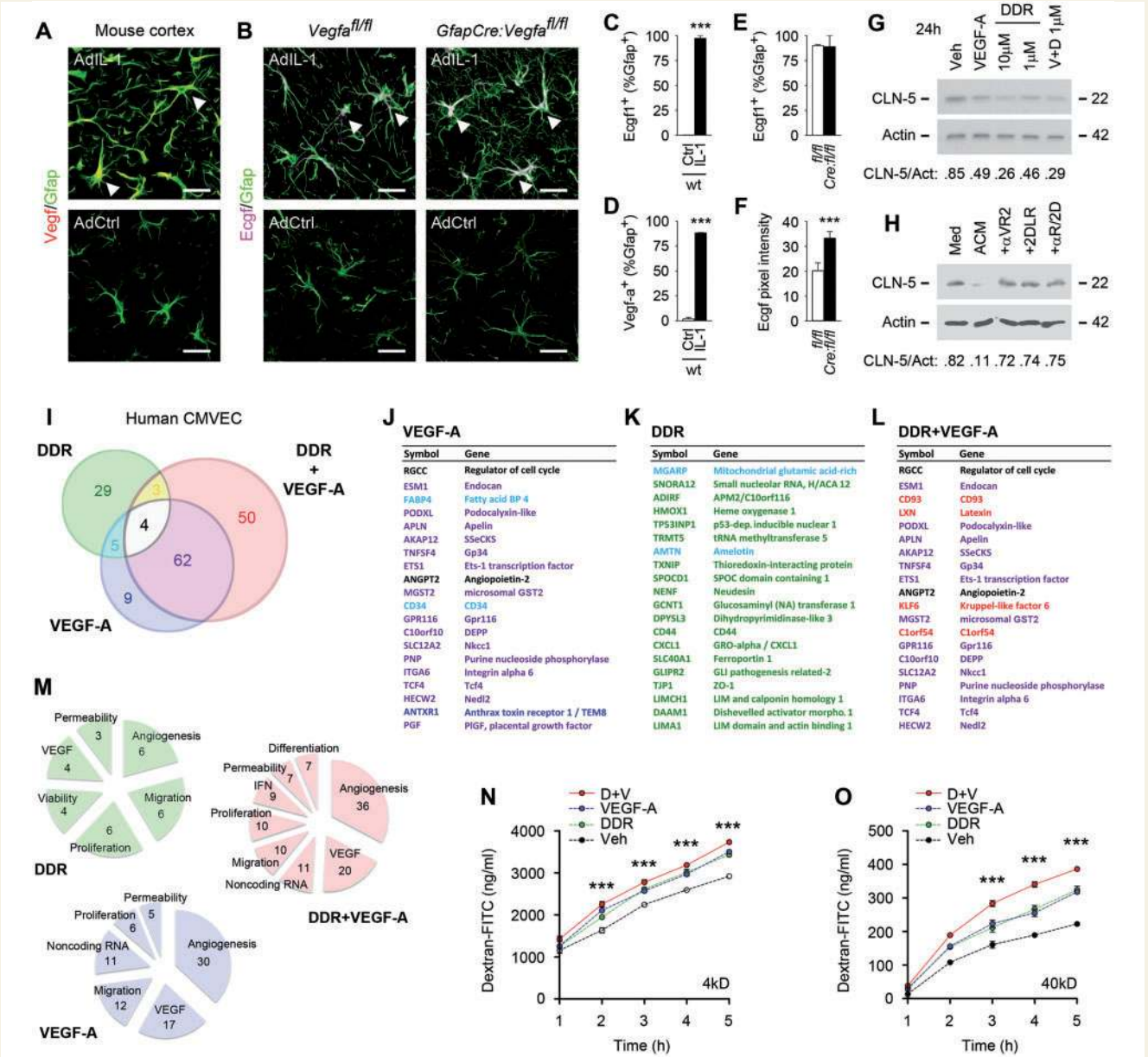

Figure 2 In human CNS microvascular endothelial cells, VEGFA and DDR elicit transcriptional patterns linked to plasticity and permeability. (**A–F**) Astrocyte-specific induction of TYMP and VEGFA in cortical inflammatory lesions. Results are shown from male 12-week-old wild-type or *Vegfa*$^{fl/fl}$ control or experimental *mGfapCre:Vegfa*$^{fl/fl}$ mice receiving cortical microinjection of 10^7 pfu AdIL-1 or AdCtrl, and sacrificed at 7 days post-induction. Sections have been stained for TYMP (ECGF1), VEGFA and lineage markers, and analysed by morphometry. TYMP or VEGFA are both specifically induced in reactive astrocytes in AdIL-1 lesions at 7 days post-induction in wild-type or non-*Cre Vegfa*$^{fl/fl}$ controls (**A–E**). Moreover, astrocytic TYMP (Ecgf1/TP) induction is significantly potentiated in *mGfapCre:Vegfa*$^{fl/fl}$ mice: pixel intensity of TYMP expression is significantly increased in *mGfapCre:Vegfa*$^{fl/fl}$ mice compared to *Vegfa*$^{fl/fl}$ controls (**B** and **F**). See also Supplementary Fig. 1C–E for panels showing data from individual channels (**C–F**). (**G**) Immunoblotting of human CMVEC treated with the TYMP product DDR (1–10 µM), VEGFA (100 ng/ml), or both, and harvested at 24 h. Data have been subjected to densitometry and results normalized to actin loading control. DDR and VEGFA each downregulate CLDN5 (**G**). Using both factors together produces stronger downregulation. Similar data showing downregulation of OCLN are illustrated in Supplementary Fig. 1F. (**H**) Treatment of human CMVEC with astrocyte conditioned medium recapitulates downregulation of CLDN5 seen with addition of VEGFA + DDR, and this decrease is blocked by αVEGFA receptor 2 (αVR2) blocking antibody, and by the DDR competitive inhibitor 2DLR, used at concentrations described in the 'Materials and methods' section. (**I–M**) Results of Illumina HumanHT-12 v4 Beadchip© transcriptional profiling of human CMVEC treated with 1 µM/130 ng/ml DDR and/or 100 ng/ml VEGFA for 24 h. Data from three separate cultures per condition were filtered as regulated by $>\log_2$ 0.5-fold and were statistically significant using Student's *t*-test with FDR correction $P < 0.05$. Results are presented as a colour-coded schematic in **I**. The 20 most strongly induced transcripts for each condition are shown in **J–L**, and all regulated transcripts and their associated functions are listed in Supplementary Tables 1–3, similarly colour-coded. Functions of regulated transcripts are summarized in **M**. These data reveal that DDR and VEGFA downregulation of endothelial tight junction proteins represents part of a wider transcriptional pattern indicative of endothelial plasticity/remodelling. VEGFA

(continued)

Table 3). Strongly suggesting that VEGFA induces endothelial plasticity, VEGFA regulated fully 30 transcripts implicated in angiogenesis, including 4 of the 10 most strongly-induced genes: ESM1, *FABP4*, *APLN* and the transcription factor *ETS1* (Sato *et al.*, 2001; Cox *et al.*, 2006; Roudnicky *et al.*, 2013; Harjes *et al.*, 2014) (Fig. 2I, J, M and Supplementary Table 1). VEGFA also modulated 12 genes linked to endothelial migration, including 5 of the 20 most strongly induced transcripts: *PODXL*, GP34 (now known as *TNFSF4*), *CD34*, *GPR116* and anthrax toxin receptor *ANTXR1* (Kunitomi *et al.*, 2000; Hotchkiss *et al.*, 2005; Larrucea *et al.*, 2008; Nielsen and McNagny, 2008; Tang *et al.*, 2013). Critically, VEGFA also regulated transcripts shown to control endothelial permeability, including the scaffold SSeCKS (now known as *AKAP12*), permeability factor angiopoietin-2, *MGST2*, and the Wnt effectors *TCF4* and β-catenin (Sjostrom *et al.*, 2001; Lee *et al.*, 2003; Nag *et al.*, 2005; Tanaka *et al.*, 2010; Engelhardt and Liebner, 2014) (Fig. 2I, J, M and Supplementary Table 1). An unexpected VEGF-sensitive function was also detected, that of downregulation of small non-coding (sn)RNAs (11 genes). As these serve to limit mRNA stability (Yin *et al.*, 2014), we hypothesized that this mechanism may enhance VEGFA-induced gene expression.

The pattern induced by DDR was also indicative of plasticity, with 29 of 41 transcripts previously connected to angiogenesis, migration, proliferation, viability or permeability (Fig.2I, K, M and Supplementary Table 2). Six genes functioning in angiogenesis were amongst the DDR-sensitive cohort, including 4 in the 20 most strongly-induced transcripts: *HMOX1*, *TXNIP*, the chemokine *CXCL1* and Wnt-associated Disheveled activator *DAAM1* (Dulak *et al.*, 2004; Caunt *et al.*, 2006; Ju *et al.*, 2010; Abdelsaid *et al.*, 2013; Park *et al.*, 2013), but just one angiogenesis-linked transcript (*FABP4*) was both VEGFA- and DDR-sensitive (Fig. 2J, K and Supplementary Tables 1 and 2). Similarly, five genes implicated in migration were DDR-regulated: *GCNT1*, *CD44*, *LIMA1*, *CD34* and integrin α10 (*ITGA10*) (Wenke *et al.*, 2006; Abe and Takeichi, 2008; Flynn *et al.*, 2013; Nolz and Harty, 2014), but only CD34 was also VEGFA-regulated (Fig. 2J, K and Supplementary Tables 1 and 2). Overall, of the 80 VEGFA- versus 41 DDR-sensitive transcripts, only nine were shared, thus the two programs were distinct but complementary, suggesting functional convergence (Fig. 2J, K, M and Supplementary Tables 1 and 2).

Importantly, the transcriptional profile produced by DDR + VEGFA co-treatment included a novel cohort of 50 uniquely co-regulated genes (Fig. 2I). Of the remaining 69, 66 were shared with the VEGFA and seven with the DDR cohort, with four regulated by each of the two factors: the regulator of proliferation *RGCC*, angiopoietin 2, the angiogenic serotonin receptor *HTR2B*, and TGF/BMP superfamily growth factor *GDF3* (Badea *et al.*, 2002; Nag *et al.*, 2005; Peiffer *et al.*, 2007; Asada *et al.*, 2009). The 50 new genes in the co-treated cohort included regulators of angiogenesis, proliferation, permeability, and differentiation (Fig. 2I, L, M and Supplementary Table 3). An additional, novel functional group was also detected, that of inhibition of interferon signalling (nine genes) (Fig. 2M and Supplementary Table 3). We hypothesized that this function may serve to enhance endothelial remodelling, as interferons have been shown to limit angiogenesis (Huang *et al.*, 2002).

Collectively, these results revealed that DDR and VEGFA both downregulate endothelial tight junction proteins, and suggested this represents part of a wider plasticity response. DDR and VEGFA induce distinct transcriptional patterns in CNS endothelium indicative of angiogenesis, permeability, migration, proliferation and/or differentiation. Furthermore, exposure to both produces a cohort of 50 uniquely co-regulated transcripts that are not significantly responsive to either alone, suggesting the potential for combinatorial functional outcomes.

DDR and VEGFA function together to induce permeability in CNS endothelia

Studies in CMVEC identified diverse functional consequences of these transcriptional programs, in terms of permeability, and plasticity more widely. Moreover, these studies confirmed combinatorial outcomes resulting from exposure to DDR and VEGFA together.

Initially we assayed endothelial permeability using a model system in which CMVEC are plated onto 0.4-μm pore inserts and left to mature and develop functional tight junctions over 14 days (Argaw *et al.*, 2006, 2009). Changes in paracellular integrity are then monitored using measurements of transendothelial passage of fluorescent dextrans of different sizes (Argaw *et al.*, 2009). We found that DDR and VEGFA each induced a significant increase in passage

Figure 2 Continued

regulates 80 genes, whereas the DDR-regulated profile is more limited, at 41 genes. Co-treatment produces a larger cohort of 119 genes. The patterns induced by VEGFA and DDR are distinct but both factors regulate cohorts implicated in angiogenesis, migration, proliferation and permeability, suggesting functional convergence. Indicative of combinatorial outcomes, co-treatment produces a novel cohort of 50 genes not regulated by either factor alone. (**N** and **O**) DDR and VEGFA function together to induce permeability in CNS endothelia. Data are shown for passage of 4 kD (**N**) and 40 kD (**O**) dextran-FITC across confluent human CMVEC monolayers on 0.4-μm pore inserts, treated with 1 μM DDR and/or 100 ng/ml VEGFA for 24 h. Each induces a significant increase in transendothelial passage of dextran-FITC over time. Both factors in combination produce greater permeability. Data in **A–F** are representative of findings from at least four mice per condition. Results in **I–M** are representative of at least three independent studies. Statistics: **C–F** = Student's *t*-test; **I–M** = Student's *t*-test with FDR correction $P < 0.05$; **N** and **O** = two-way ANOVA plus Bonferroni post-test. Scale bars in **A** and **B** = 30 μm.

of both 4 kD and 40 kD dextran-FITC through the monolayer over time (Fig. 2N and O). Moreover, and importantly, using both together produced a significantly more potent effect (Fig. 2N and O).

VEGFA and DDR collaboratively promote CMVEC proliferation, motility and angiogenesis

Further functional analyses supported the hypothesis that effects of DDR and VEGFA on permeability represent part of a wider program of endothelial remodelling (Fig. 3). BrdU labelling and caspase cleavage assays demonstrated that both DDR and VEGFA significantly increased proliferation and reduced apoptosis in human CMVEC cultures, although using both together did not produce additive effects (Fig. 3A and B). Conversely, we did observe enhanced outcomes of combined treatment in assays of motility and angiogenesis. In scratch-wound closure assays, we stimulated motility and migration by producing a linear 500-μm diameter wound in a confluent CMVEC monolayer (John *et al.*, 2004), then compared effects of DDR and/or VEGFA on rates of wound closure (Fig. 3C and D). CMVEC in control cultures closed the 500 μm gap in 24 h, and were confluent by 36 h (data not shown). Conversely, closure was substantially accelerated in DDR- or VEGFA-treated cultures, and further increased in co-treated cultures, such that only a 30-μm gap remained in co-treated cultures at 16 h, versus 130 μm in controls (Fig. 3C and D). In more complex angiogenesis assays, we plated CMVEC onto a gel substrate and examined responses to DDR and/or VEGFA. While controls remained confluent and quiescent, cultures treated with DDR or VEGFA formed tubular structures resembling capillaries over a 24-h period, and notably, co-treatment potentiated tube formation (Fig. 3E and F).

These data showed that DDR and VEGFA induce permeability in CMVEC cultures and suggest that this represents part of a wider program of endothelial remodelling in inflammatory lesions. In addition, these studies confirmed additive or combinatorial functional effects of DDR and VEGFA in assays of permeability, migration/motility and angiogenesis.

DDR and VEGFA act in combination to induce blood–brain barrier breakdown *in vivo*

To compare effects of DDR and VEGFA on the blood–brain barrier, we delivered $VEGFA_{165}$ [60 ng in 3 μl phosphate-buffered saline (PBS)/bovine serum albumin] and/or DDR (400 ng in 3 μl PBS) or vehicle control stereotactically

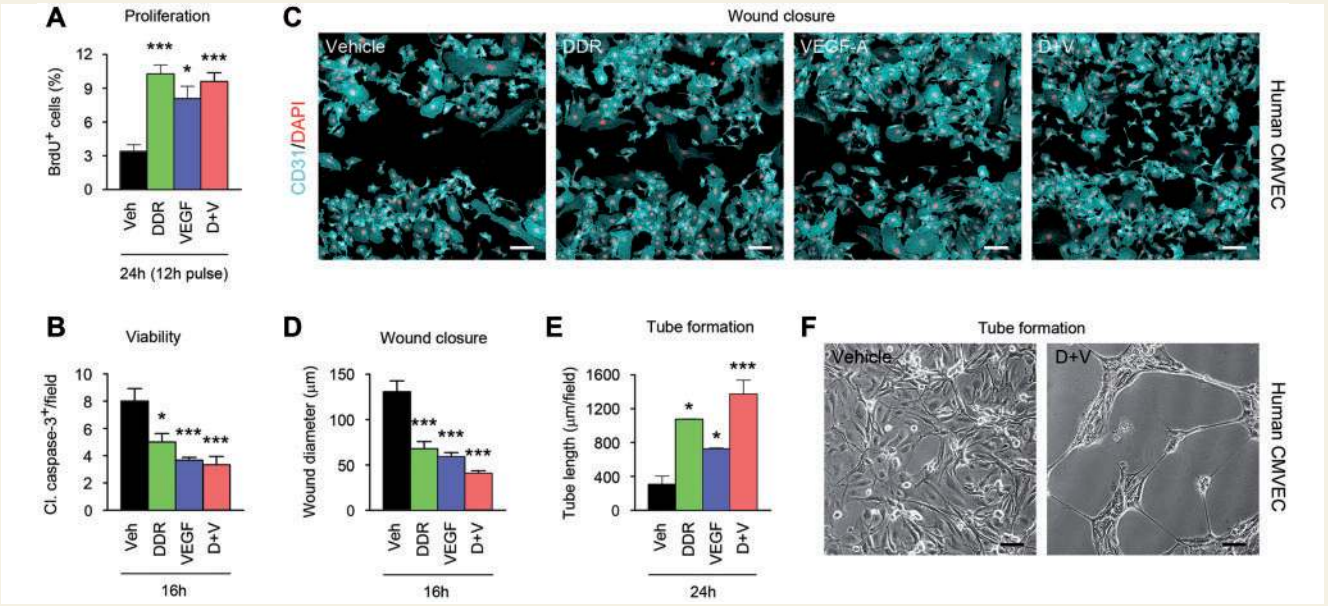

Figure 3 DDR and VEGFA together promote motility and angiogenesis in CMVEC cultures. Results of functional studies in human CMVEC cultures treated with 100 ng/ml VEGFA and/or 1 μM/130 ng/ml DDR or vehicle control, then subjected to assays of proliferation (BrdU incorporation, **A**), viability (cleaved caspase-3 staining, **B**), motility/migration (scratch-wound closure, **C** and **D**), and angiogenesis (tube formation, **E** and **F**) over 16–24 h as described in the text. (**A**) Proliferating ($BrdU^+$) cells are increased in CMVEC treated with DDR or VEGFA. No additive effect is observed in co-treated cultures. (**B**) VEGFA and DDR also both reduce numbers of apoptotic (cleaved caspase-3^+) cells in CMVEC cultures, but co-treatment has no additional impact. (**C** and **D**) DDR and VEGFA independently accelerate wound closure in a CMVEC scratch-wound assay. In combination they produce a stronger outcome, such that at 16 h only a 30-μm gap remains in co-treated cultures, versus 130 μm in controls. (**E** and **F**) In more complex angiogenesis assays, CMVEC cultures form tubular structures over 24 h in response to VEGFA or DDR, and this effect is potentiated by co-treatment. Results in all panels are representative of at least three independent experiments. Statistics: **A**, **B**, **D** and **E** = ANOVA plus Bonferroni post-test, $*P < 0.05$, $***P < 0.001$. Scale bars in **C** and **F** = 25 μm.

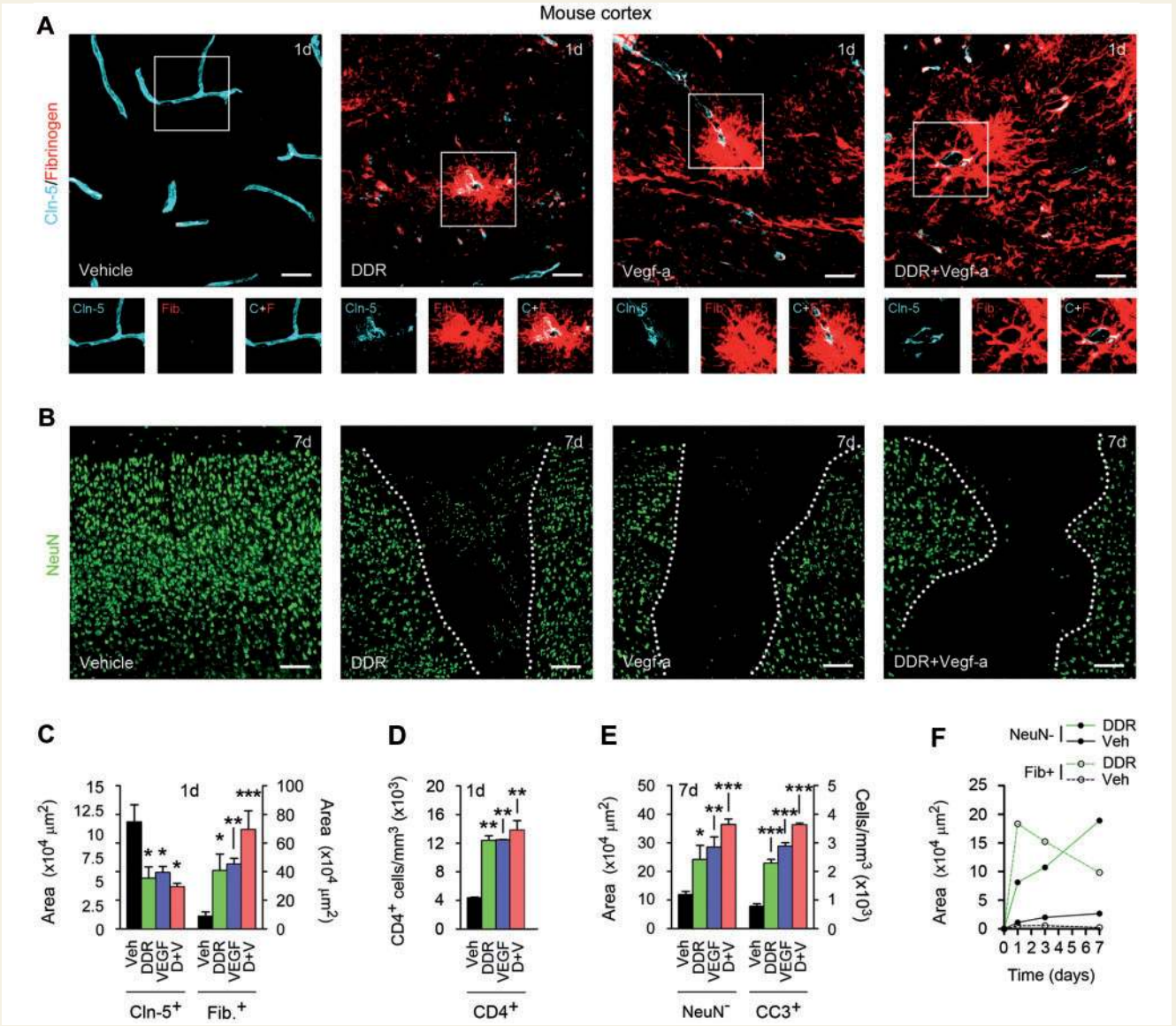

Figure 4 DDR and VEGFA co-operate to produce blood–brain barrier breakdown *in vivo*. (**A** and **B**) Confocal *Z*-series projections of cerebral cortices of 12-week-old C57BL/6 mice 24 h (**A**) or 7 days (**B**) following stereotactic microinjection of murine $VEGFA_{165}$ (60 ng in 3 µl PBS/BSA), and/or DDR (400 ng in 3 µl PBS), or vehicle control. Sections in (**A**) are immunostained for the endothelial tight junctions protein CLDN5 (blue channel) plus fibrinogen as a marker of blood–brain barrier breakdown (red channel). Both channels from areas outlined are shown below. Sections in **B** are stained for the neuronal marker NeuN (green channel). Morphometrically analysed data are presented in **C–E**. Blood–brain barrier disruption is seen around vessels in VEGF- or DDR-injected regions, and CLDN5 immuno-reactivity in these areas is reduced and discontinuous (**A** and **C**). These changes are associated with lymphocyte infiltration into VEGF- or DDR-injected locales (**D**). Blood–brain barrier breakdown is notably exacerbated in mice receiving $VEGFA_{165}$ plus DDR together (**A** and **C**). Blood–brain barrier disruption in areas receiving $VEGFA_{165}$ and/or DDR is followed by neuronal loss, and with the presence of apoptotic cleaved caspase-3^+ $NeuN^+$ neurons. These effects are also exacerbated in mice receiving $VEGFA_{165}$ plus DDR in combination (**B** and **E**). (**F**) Time course morphometric measurements over a 7-day period post-injection reveals that blood–brain barrier disruption, as defined by the increase in area of parenchymal fibrinogen positivity, precedes neuronal loss (increase in area of $NeuN^-$ field) in DDR-induced lesions. Similar data are shown for $VEGFA_{165}$-induced lesions in Supplementary Fig. 2A, which additionally demonstrates that co-treatment results in more persistent blood–brain barrier breakdown. Statistics: **C–E** = ANOVA plus Bonferroni post-test, $^*P < 0.05$, $^{**}P < 0.01$, $^{***}P < 0.001$. Scale bars in **A** and **B** = 50 µm. Data shown are representative of findings from at least four mice per condition per time point.

into the left cerebral cortex of adult mice (Argaw *et al.*, 2006), then measured changes in barrier function over 24 h to 7 days post-induction (Fig. 4 and Supplementary Fig. 2). Using morphometric analysis of confocal image stacks, we quantified sections immunostained for CLDN5 as a known marker of blood–brain barrier integrity, the T helper lymphocyte marker CD4 as an indication of parenchymal leucocyte infiltration, and the serum proteins

fibrinogen or albumin, which are normally confined to the vasculature but enter the CNS parenchyma upon blood–brain barrier opening (Argaw *et al.*, 2006).

Minimal blood–brain barrier disruption was observed in vehicle controls, and CLDN5 immunoreactivity in microvascular endothelium was smooth and continuous (Fig. 4A), compatible with published data for CLDN5, OCLN and other CNS endothelial tight junction markers such as zona occludens 1 (now known as TJP1) (Argaw *et al.*, 2009, 2012; Li *et al.*, 2010). Numbers and organization of cortical $NeuN^+$ neurons were normal, with no apoptosis detected (Fig. 4B). However, at 24 and 48 h we observed blood–brain barrier breakdown (measured by parenchymal fibrinogen and albumin immunoreactivity) in DDR- or $VEGFA_{165}$-injected areas, perivascularly and extending deeper into the parenchyma (Fig. 4A and C, 24 h post-injection illustrated). Endothelial CLDN5 staining in areas of blood–brain barrier disruption appeared patchy and discontinuous, in both DDR-injected and VEGFA-injected samples (Fig. 4A and C), and these changes were accompanied by parenchymal accumulation of $CD4^+$ cells (Fig. 4D). Importantly, blood–brain barrier disruption, as measured by serum protein extravasation, was exacerbated in mice receiving DDR and $VEGFA_{165}$ together (Fig. 4A and C).

We have previously shown that the consequences of blood–brain barrier breakdown contribute to neuro-pathology (Argaw *et al.*, 2012), and so we measured neuronal injury in DDR- and/or $VEGFA_{165}$-induced cortical lesions. Similar to results for $VEGFA_{165}$ (Argaw *et al.*, 2012), in samples receiving DDR we observed neuronal loss in areas of blood–brain barrier disruption at 7 days post-induction (Fig. 4B and E), and apoptotic cleaved caspase-3^+ $NeuN^+$ neurons were present at the borders of these areas (Fig. 4E). Further investigation revealed that blood–brain barrier disruption in response to DDR or $VEGFA_{165}$ was maximal at 24 h, then declined over the course of 7 days post-induction, whereas neuronal injury, detectable at low levels at 24 h, continued to increase to 7 days post-induction, demonstrating that neuronal loss occurs subsequent to blood–brain barrier disruption (Fig. 4F and Supplementary Fig. 2A). Notably, treating with both DDR and $VEGFA_{165}$ together led to more extensive and persistent blood–brain barrier breakdown, and significantly more extensive neuronal loss (Fig. 4B, E and Supplementary Fig. 2A).

Multiple pieces of evidence pointed to this effect being driven by blood–brain barrier breakdown. In the adult CNS, VEGFR2/KDR/FLK1 is expressed by endothelial cells but not neurons or other lineages, thus neuronal death in VEGF-induced lesions results from the consequences of loss of blood–brain barrier integrity (Argaw *et al.*, 2009). Suggesting that blood–brain barrier disruption is also at the root of neuropathology in DDR-induced lesions, we detected no apoptosis or reduction in cell number in CMVEC or neuronal cultures exposed to DDR concentrations used in our studies—rather, these levels produced anti-apoptotic effects (Fig. 3B and Supplementary Fig. 2B and C). Moreover, previous reports have shown that effects of DDR on viability would require concentrations at least a thousand times higher, similar to the high concentrations required to see detrimental effects of ribose or arabinose (Kletsas *et al.*, 1998).

Together, these studies showed that, similar to VEGFA, DDR induces blood–brain barrier breakdown in the adult CNS. Moreover, DDR and VEGFA in combination produce more severe and persistent blood–brain barrier opening. The consequences of these effects are associated with subsequent neuronal loss and apoptosis in grey matter lesions.

In EAE, TYMP induction correlates with blood–brain barrier breakdown and endothelial CLDN5 disruption

To directly examine functional relevance to inflammatory CNS disease, we initially examined samples from mice with the multiple sclerosis model EAE (Fig. 5 and Supplementary Fig. 2D–G). Disease was induced in 8-week-old C57BL/6 males using $MOG_{35–55}$ as described (Gurfein *et al.*, 2009). Progressive ascending paralysis was apparent from 10–12 days, and was evaluated on a widely-used 5-point scale (Gurfein *et al.*, 2009). Mice showing paraparesis or paraplegia (score 2–3) were sacrificed at 15–18 days, and serial sections of lumbar spinal cord stained for TYMP, VEGFA and GFAP, plus CLDN5, fibrinogen, albumin and inflammatory cell markers. Immunoreactivity in random fields of lumbar spinal cord white matter was quantified by a blinded observer using morphometry.

Importantly, these analyses demonstrated co-induction of TYMP and VEGFA in EAE lesions, which correlated with downregulation of CLDN5, blood–brain barrier breakdown and parenchymal leucocyte entry. We observed inflammatory spinal cord white matter lesions in mice with EAE, as previously characterized (Gurfein *et al.*, 2009). These encompassed perivascular accumulation of $CD45^+$ inflammatory cells, and CNS demyelination and oligodendrocyte loss (Supplementary Fig. 2D). Blood–brain barrier breakdown in lesions was extensive, as assessed by parenchymal entry of fibrinogen and albumin, and disruption of CLDN5 (Fig. 5A). Furthermore, confocal imaging confirmed invasion of $CD4^+$ T helper lymphocytes into the CNS parenchyma, across the blood–brain barrier and glia limitans as identified by pan-laminin staining (Fig. 5B). Importantly, both TYMP and VEGFA were strongly and specifically induced in reactive astrocytes in EAE lesions, with each localizing to >90% $GFAP^+$ cells (Fig. 5C–E). Moreover, morphometric analysis confirmed that in EAE samples, TYMP expression correlated strongly with blood–brain barrier breakdown and reduced CLDN5 immunoreactivity (Fig. 5F–H) and with T lymphocyte entry (Fig. 5I and J), similar to the patterns seen for VEGFA induction (Fig. 5K–O), which were also compatible with previous data (Argaw *et al.*, 2009). TYMP induction

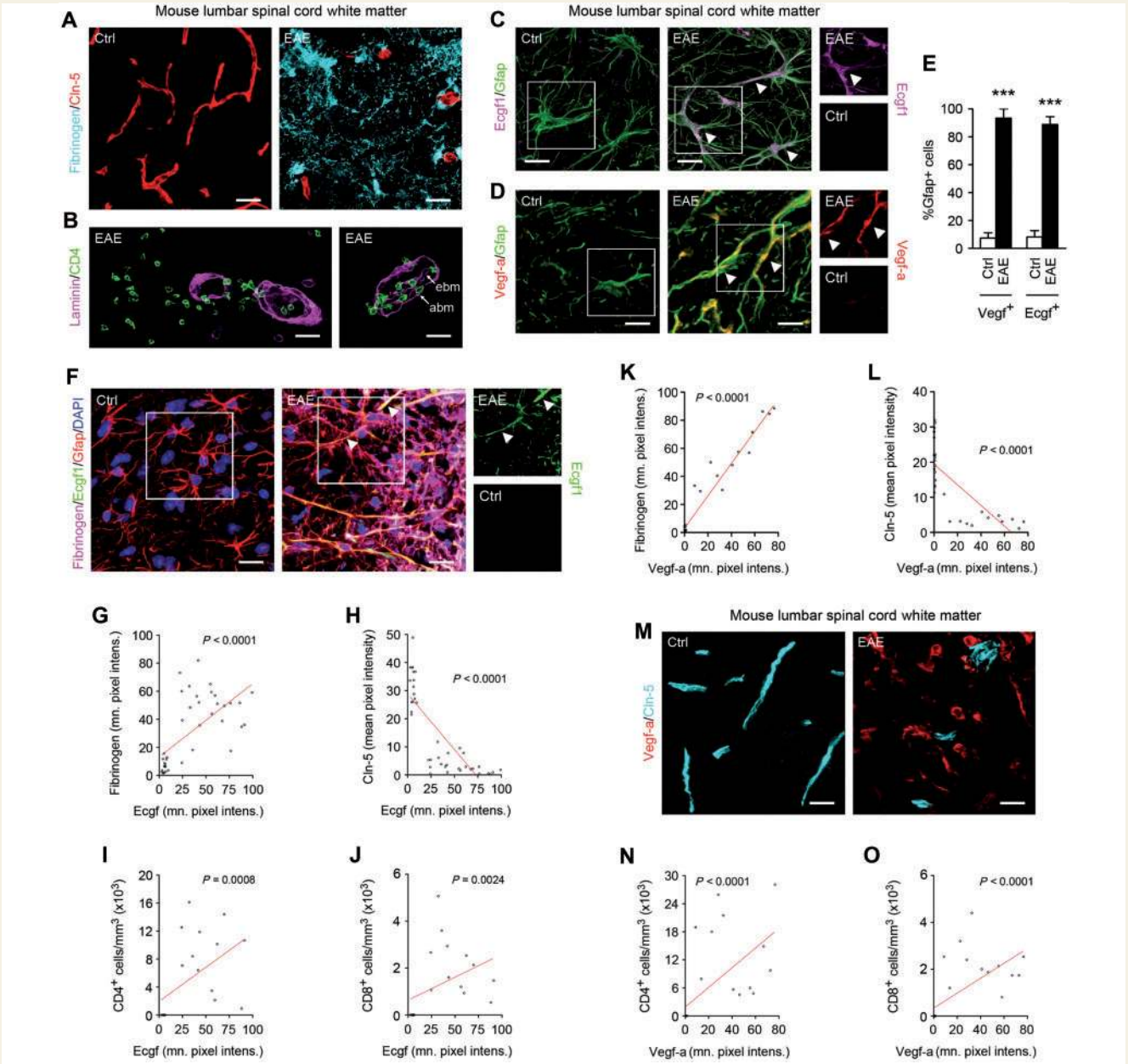

Figure 5 Astrocytic TYMP is upregulated in EAE lesions, and correlates with blood–brain barrier disruption and leucocyte infiltration. (**A–D**) Confocal *Z*-series projections of ventrolateral lumbar spinal cord from 10-week-old C57BL/6 mice with EAE (tail paralysis + paraparesis) 15–18 days post-induction, or age-and sex-matched controls. Sections are immunostained for fibrinogen + CLDN5 (**A**), CD4 + pan-laminin (**B**), or TYMP or VEGFA plus the reactive astroglial marker GFAP (**C** and **D**). Morphometric analysis of TYMP and VEGFA expression in lesions is shown in **E**. Additional features of EAE pathology are illustrated in Supplementary Fig. 2D. EAE sections display disruption of the blood–brain barrier in lesions, as assessed by parenchymal immunoreactivity for fibrinogen and reduced endothelial CLDN5 immunoreactivity (**A**). (**B**) Furthermore, lesions additionally display inflammatory cell invasion into the CNS parenchyma, across the blood–brain barrier and glia limitans as demarcated by pan-laminin staining, which labels the endothelial and astrocytic basement membranes (ebm, abm, arrowed in *right* panel). Importantly, lesions are also strongly positive for TYMP and VEGFA (**C** and **D**, representative areas arrowed), which both localize specifically to and are expressed almost universally by GFAP$^+$ reactive astrocytes (**E**). In (**C** and **D**), TYMP (Ecgf1) and VEGFA immmunoreactivity in areas outlined are shown as single channels to the right of the main panels. (**F–O**) Morphometric analysis of spinal cord sections from mice with EAE, immunostained for fibrinogen, CLDN5 and markers for the T helper and T cytotoxic lymphocyte subsets (CD4 and CD8, respectively), plus TYMP (**F–J**) or VEGFA (**K–O**). Examples of EAE and control sections stained for TYMP (Ecgf1) + fibrinogen + CLDN5, or VEGFA + CLDN5, are shown in **F** and **M**. These analyses demonstrate that TYMP expression is positively correlated with extravasation of fibrinogen and negatively correlated with endothelial CLDN5 expression (**F–H**). TYMP also correlates positively with infiltration of CD4$^+$ and CD8$^+$ lymphocytes into the parenchyma (**I** and **J**). Similarly, VEGFA is also positively correlated with intraparenchymal fibrinogen and CD4$^+$ and CD8$^+$ lymphocyte infiltration, and negatively correlated with CLDN5 (**K–O**). Additional images relevant to findings in (**F–O**) are presented in Supplementary Fig. 2E–G. Data in all panels are representative of at least three animals per condition per experiment, and at least three independent studies. Statistics: **E** = Student's *t*-test; **G–L**, **N** and **O** = Spearman rank correlation, ***$P < 0.001$. Scale bars in **A** and **M** = 30 μm; in **B–D** and **F** = 15 μm.

also correlated with upregulation of the reactive astrocyte marker GFAP (Supplementary Fig. 2E). Importantly, however, illustrating specificity of the TYMP and VEGFA findings, GFAP upregulation did not correlate significantly with blood–brain barrier breakdown or CLDN5 downregulation (Supplementary Fig. 2F and G).

Collectively, these results showed correlation between TYMP and VEGFA induction and blood–brain barrier breakdown and lymphocyte entry, and reduced CLDN5 immunoreactivity, in a multiple sclerosis model.

In human multiple sclerosis white matter lesions, TYMP and VEGFA localize specifically to reactive astrocytes

Importantly, analysis of lesion samples from multiple sclerosis patients confirmed relevance of these findings to human disease. To assess whether TYMP and VEGFA are present in human multiple sclerosis white matter lesions, we performed immunohistochemical staining in normal and lesional areas of human brain tissue from patients with multiple sclerosis and other neurological disease and normal age- and sex-matched controls (Supplementary Fig. 3 and Supplementary Table 4). Supplementary Fig. 3A shows a low magnification image of a chronic active multiple sclerosis lesion centred on a vessel in a 32-year-old female patient, stained with Luxol Fast blue, whereas Supplementary Fig. 3B–E show higher magnification images stained with Luxol Fast blue and for MBP to illustrate demyelination (Supplementary Fig. 3B and C), and with haematoxylin and eosin to illustrate pathology (Supplementary Fig. 3D), and for TYMP (Supplementary Fig. 3E). Compatible with previous studies (Zhang *et al.*, 2006), the border of the lesion was active and hypercellular, and contained some abnormal and fragmented myelin, although the lesion centre was fully demyelinated (Supplementary Fig. 3A–C). At this active border, a major site of blood–brain barrier disruption in MRI studies (Absinta *et al.*, 2013), and to a lesser extent within the lesion, were large, hypertrophic cells with morphology matching that of reactive astrocytes (Supplementary Fig. 3D). Importantly, TYMP immunoreactivity also localized to these hypertrophic cells, within the lesion and particularly at the border (Supplementary Fig. 3E). Supplementary Fig. 3F–J show high magnification images of individual cells immunostained for TYMP, VEGFA, IL-1 and cell lineage markers. Higher magnification analysis confirmed TYMP localization to hypertrophic cells with morphology corresponding to that of reactive astrocytes (Supplementary Fig. 3F), which were also positive for GFAP (Supplementary Fig. 3G). Compatible with previous reports (Proescholdt *et al.*, 2002; Argaw *et al.*, 2006), VEGFA also localized specifically to reactive astrocytes in active areas of multiple sclerosis lesions (Supplementary Fig. 3H), but not in adjacent normal-appearing white matter. Neither TYMP nor VEGFA was expressed in normal control tissue. Also matching previous data (Brosnan *et al.*, 1995), IL-1 localized to cells with the typical morphology characteristic of $RCA1^+$ macrophages and microglia (Supplementary Fig. 3I and J). Immunoreactivity for IL-1 was not observed in normal control tissue. Isotype and primary antibody omission controls were also performed, and were found to be negative.

Blockade of VEGFA and TYMP signalling protects against blood–brain barrier opening and paralysis in EAE

We compared the impact of TYMP blockade on disease severity in EAE with that of inhibition of VEGFA signalling, and tested the outcome of blocking both pathways in combination (Fig. 6). We sensitized mice (eight per group) as above (Gurfein *et al.*, 2009), then from onset of weight loss (>10% body weight) treated them daily for 7 days with the DDR inhibitor 2DLR (20 mg/kg/d), and/or cavtratin, a selective inhibitor of VEGFA signalling (2.5 mg/kg/d) (Argaw *et al.*, 2012). We have previously shown that in EAE, cavtratin treatment closely mimics the effects of astrocyte-specific *Vegfa* inactivation (Argaw *et al.*, 2012). Neurological signs and pathology were evaluated as above.

Weight loss (and onset of therapy) occurred at 7 days post-sensitization, and ascending paralysis was first observed 24 h later, with severity in controls increasing until 17 days, when neurologic deficit reached a plateau at a mean score of 3.875, indicating severe disease with complete hindlimb paralysis plus mild forelimb weakness (Fig. 6A). Signs in 2DLR-treated mice were much milder, peaking at 17 days at a mean score of just 1.875, indicative of a limp tail with minor hindlimb weakness. Notably, this reduction in paralysis was similar to that seen in cavtratin-treated mice, which reached a mean score of 2.07, reflecting a limp tail with hindlimb weakness. For both treatment regimens, differences in disease severity were highly significant at 13–21 days compared with vehicle controls (Fig. 6A). Comparison of peak clinical severity in each individual in all three groups was even more revealing. Almost all controls (87.5%) but only 25% of 2DLR-treated and 15% of the cavtratin-treated mice displayed complete hindlimb paralysis or worse (score $\geqslant$3) (Fig. 6B). Moreover, in controls, mortality or severe paralysis requiring euthanasia (score $\geqslant$4) was 50%, whereas in the cavtratin-treated group it was only 15%. Strikingly, no mortality at all was encountered in the 2DLR-treated cohort (Fig. 6B).

These improvements in clinical disease were associated with reduced blood–brain barrier breakdown in lesions in 2DLR-treated mice (Fig. 6C and D), maintenance of CLDN5 expression (Fig. 6C and E), and decreased inflammatory cell infiltration (Fig. 6F–H). Importantly, these changes were associated with reduced tissue damage, in terms of decreased demyelination and improved oligodendrocyte and axonal preservation (Fig. 6I–K). Notably, the extent of protection provided by 2DLR was similar to

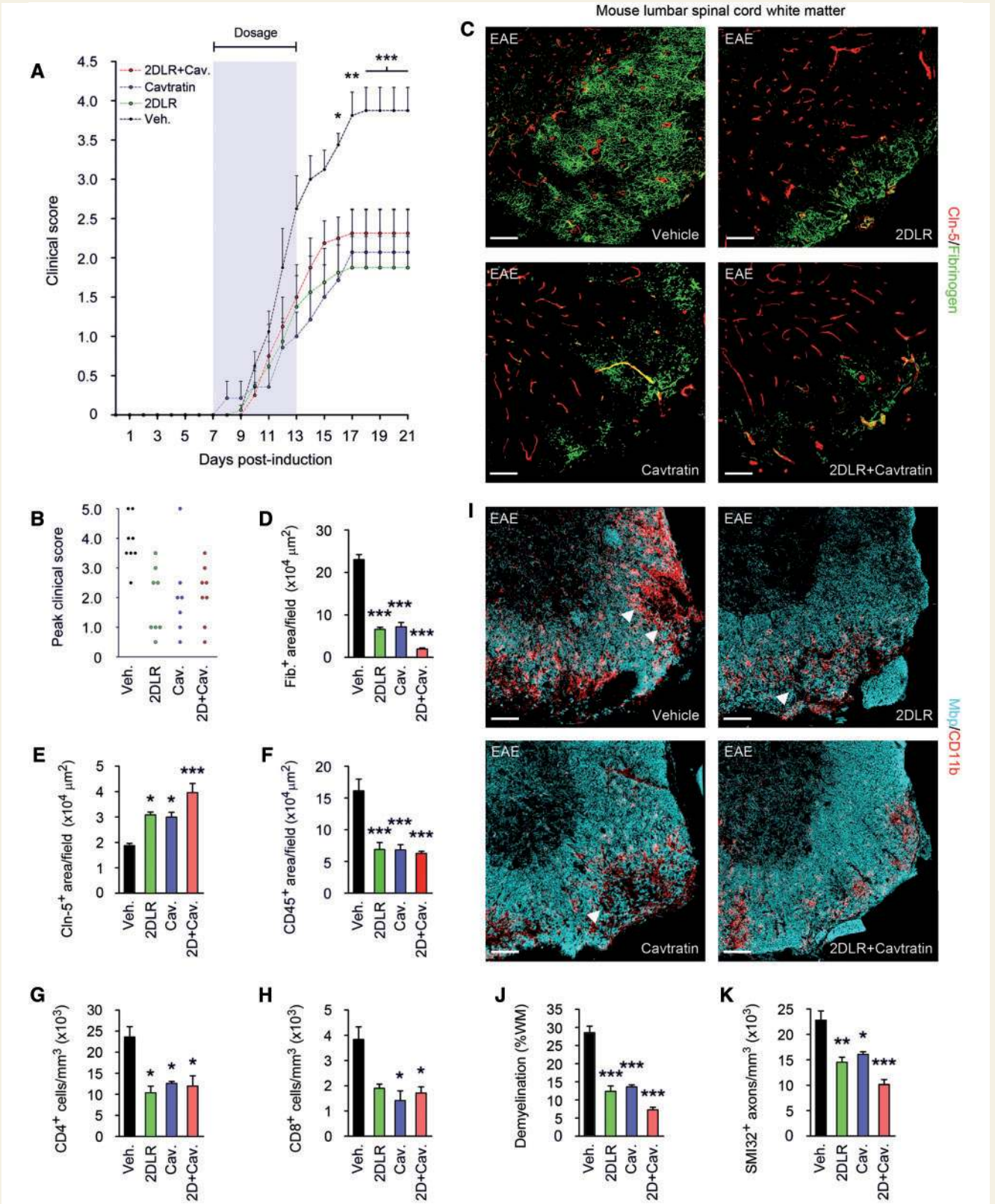

Figure 6 Blockade of VEGFA and TYMP signalling reduces paralysis and tissue damage in EAE. (**A**) Mean clinical scores are shown from mice (8-week-old male C57BL/6, eight per group) sensitized with $MOG_{35–55}$/CFA, then from onset of weight loss (7 days post-induction) treated for 7 days with 20 mg/kg/day 2DLR, and/or 2.5 mg/kg/day the inhibitor of VEGFA signalling, cavtratin, or vehicle control (shaded area). Neurological deficit has been scored daily for each animal according to a widely-used 5-point scale (EAE scoring: 1 limp tail; 2 limp tail and weakness of hind limb; 3 limp tail and complete paralysis of hind legs; 4 limp tail, complete hind leg and partial front leg paralysis) (Gurfein *et al.*, 2009). Ascending paralysis is observed in all groups from 8 days post-induction, increasing in controls until signs stabilize at 17 days post-induction

(continued)

that produced by cavtratin treatment (Fig. 6C–K). No differences in lymphocyte numbers were seen in peripheral lymphoid organs of mice treated with either 2DLR or cavtratin, versus vehicle controls (data not shown).

Importantly, blocking TYMP and VEGFA together using 2DLR plus cavtratin produced enhanced neuroprotection in co-treated mice. Interestingly, combination therapy did not produce additional benefits in terms of acute disability scores (Fig. 6A and B). Cavtratin at the doses used in these studies produces outcomes similar to astrocytic *Vegfa* inactivation (Argaw *et al.*, 2012), and additionally blocking TYMP did not further enhance clinical outcome. We hypothesized that abrogation of blood–brain barrier breakdown may reach a maximal level of impact on clinical disability in the acute stages of autoimmune demyelination. However, examination of spinal cord samples did reveal additional improvements in blood–brain barrier integrity in co-treated mice (Fig. 6C–E), although lymphocyte infiltration was not significantly affected (Fig. 6F–H). Importantly, this improvement in blood–brain barrier integrity was also associated with greater myelin and axon preservation than that produced by blockade of either TYMP or VEGFA alone, outcomes likely to impact chronic disease outcomes (Fig. 6I–K).

Collectively, the results of these studies *in vivo* implicated astrocytic TYMP as an important astrocyte-derived permeability factor in inflammatory CNS conditions. They further suggested that TYMP interacts with VEGFA to promote blood–brain barrier breakdown in a model of multiple sclerosis.

Discussion

Breakdown of the blood–brain barrier is a key pathogenic step in the initiation and progression of autoinflammatory demyelinating disease (Bruck *et al.*, 1997). Advances in understanding of the underlying mechanisms have led to strategies to minimize clinical disability and tissue damage during disease exacerbation in multiple sclerosis and neuromyelitis optica (Agrawal *et al.*, 2006; Alvarez *et al.*, 2011; Hosokawa *et al.*, 2011; Shimizu *et al.*, 2012). We recently found that the inflammatory cytokine IL1B stimulates resident astrocytes to secrete VEGFA, which acts via VEGFR2/KDR/Flk-1 and downstream NOS3 (eNOS) signalling to downregulate endothelial tight junction components at the blood–brain barrier, facilitating ingress of damaging humoral factors and leucocytes into the CNS parenchyma (Argaw *et al.*, 2009, 2012). A recent study supports a model in which VEGFA exerts its effect on blood–brain barrier disruption via a polarization-specific interaction with VEGFR2 receptors on the abluminal (CNS) side of the endothelium, whereas in contrast interactions with luminal VEGFR1 activate Akt, resulting in cytoprotection (Hudson *et al.*, 2014). Nonetheless, studies in which genetic *Vegfa* inactivation or pharmacologic blockade of VEGFR2 signalling in mice does not fully abrogate blood–brain barrier disruption or tissue damage have suggested contributions of additional pathways to blood–brain barrier opening in inflammatory lesions.

The current study is the first to identify a significant role in blood–brain barrier breakdown for the enzymatic TYMP (previously known as ECGF1/TP) pathway, which produces the diffusible signal DDR. Both VEGFA and TYMP have previously been shown to exert independent and sometimes combinatorial effects on tumour angiogenesis, depending on the malignant subtype (Toi *et al.*, 1995; Takanami *et al.*, 1997; Uchida *et al.*, 1998; Tsujitani *et al.*, 2004). An older microarray screen from our group had not previously identified this important candidate pathway at the time of VEGFA discovery, due to its absence from the previous microarray library (Argaw *et al.*, 2006). Here, our data reveal that these two signalling pathways are both implemented in driving CNS microvascular permeability. Importantly, our findings further suggest that they act together to drive blood–brain barrier opening in inflammatory lesions.

Our experiments demonstrate that IL1B stimulates human astrocytes to secrete DDR via upregulated activity of TYMP and that this induction, like that of VEGFA, requires NFκB1, but not p38 MAP kinase, and is independent of other pathways such as JAK-STAT signalling. Moreover, conditionally disabling astrocyte-specific *Vegfa* in mice leads to an increase in astrocytic TYMP induction by inflammatory cytokines, perhaps suggesting that negative feedback products of the VEGFA pathway suppress TYMP expression when present. Functionally, a

Figure 6 Continued

at a mean of 3.875, indicative of hindlimb paralysis plus mild forelimb weakness. Signs in 2DLR-treated or cavtratin-treated mice are much milder, stabilizing at 17 days at 1.875 or 2.07 (limp tail with hindlimb weakness), respectively. Interestingly, co-treatment does not produce additional clinical benefit. (**B**) Peak severity of paralysis is reduced in 2DLR-, cavtratin-, and co-treated mice. Controls (87.5%) but only 15–25% of 2DLR-, cavtratin- or co-treated mice display hindlimb paralysis or worse (score $\geqslant$3) during the disease course (21 days). Mortality or severe paralysis requiring euthanasia (score $\geqslant$4) reaches 50% in controls, but only 15% in the cavtratin-treated group, whereas mortality is absent in the 2DLR- and co-treated cohorts. (**C–K**) Neuropathological data from lumbar spinal cords of representative mice (three per group) from each cohort, sacrificed at 21 days. EAE controls display blood–brain barrier breakdown and disruption of endothelial CLDN5 (**C–E**), $CD45^+$ inflammatory cell accumulation and $CD4^+$ and $CD8^+$ lymphocyte infiltration (**F–H**), demyelination and oligodendrocyte loss, and axonal transection (**I–K**). In **I**, representative areas of demyelination are arrowed. In 2DLR- and cavtratin-treated mice, CLDN5 expression is maintained and blood–brain barrier breakdown reduced (**C–E**), and inflammatory cell accumulation and lymphocyte infiltration restricted (**F–H**). Demyelination is decreased, and axonal integrity preserved (**I–K**). Importantly, although co-treatment is not associated with additional clinical benefits, it potentiates blood–brain barrier integrity and myelin and axon preservation (**C–E** and **I–K**). Scale bars in **C** and **I** = 50 μm. Statistics: **A** = two-way ANOVA plus Bonferroni test; **D–H**, **J** and **K** = one-way ANOVA plus Bonferroni test, $^*P < 0.05$, $^{**}P < 0.01$, $^{***}P < 0.001$. Data are representative of three independent experiments.

compensatory increase in one microvascular modulator pathway (TYMP) in the absence of the other (VEGFA) indicates the potential for combinatorial actions and/or redundancy. Transcriptional and translational profiles of human CMVEC treated with VEGFA or DDR, the active metabolite of the TYMP pathway, support this hypothesis. Downregulation of CLDN5 and OCLN with associated disruption in endothelial tight junctions is a previously recognized VEGFA-induced mechanism driving CMVEC permeability, and is also induced independently by DDR in CMVEC cultures. Furthermore, VEGFA and DDR together exhibit a stronger outcome in terms of decreasing CLDN5 and OCLN levels and promoting permeability.

Interestingly, our gene expression profiling studies indicate that DDR and VEGFA downregulation of endothelial tight junction proteins represents part of a wider plasticity response, compatible with previous observations suggestive of angiogenesis in lesions in multiple sclerosis and its models (Ludwin and McFarland, 2001; Kirk *et al.*, 2004; Muramatsu *et al.*, 2012). In these BeadArray© experiments, we found that VEGFA regulates 80 genes, whereas the DDR profile of activity includes 41 genes. Co-treatment produces a larger cohort of 119 genes. Suggesting that VEGFA induces endothelial remodelling, of the 80 VEGF-regulated genes, 53 have been linked to angiogenesis, endothelial migration, proliferation and/or permeability. The pattern induced by DDR is largely composed of different genes but also indicative of plasticity, with 25 of 41 transcripts previously connected to angiogenesis, migration, proliferation, viability or permeability, thus the two programs are distinct but complementary, suggesting a functional convergence. Importantly, the third distinct transcriptional profile of 119 transcripts produced by DDR + VEGFA co-treatment includes a novel cohort of 50 uniquely co-regulated genes not induced by either factor alone, further suggesting potential for combined actions. Our functional studies *in vitro* support the idea of a wider VEGFA and/or DDR-induced response in CMVEC, revealing enhanced proliferation and viability. Moreover, co-treatment produces combinatorial outcomes in assays of both migration and angiogenesis.

Nonetheless, increased transendothelial permeability and blood–brain barrier breakdown seem to represent critical pathogenic outcomes of astrocytic VEGFA and DDR synthesis in inflammatory CNS lesions. Either factor alone is sufficient to produce these effects, as demonstrated both *in vitro* and *in vivo*. DDR and VEGFA individually induce transendothelial passage of 4 kD and 40 kD dextrans in human CMVEC cultures, and introduction of VEGFA or DDR into mouse cortex independently leads to disruption of endothelial CLDN5 expression, breakdown of the blood–brain barrier, transendothelial passage of plasma proteins and inflammatory cells into the brain parenchyma, and subsequent neuronal apoptosis and loss. The two factors together have more potent effects on these outcomes, suggesting that they have a redundant or cooperative role in autoinflammatory blood–brain barrier breakdown. Because VEGFA and DDR themselves are not toxic to isolated CMVEC or neurons in culture, the neuronal loss observed subsequent to blood–brain barrier breakdown in these experiments is likely secondary to a downstream cascade involving transvascular migration of cytotoxic cells and/or soluble factors through the blood–brain barrier.

The relevance of these pathways to disease pathogenesis is further supported by the presence of specific VEGFA and TYMP expression in reactive astrocytes in active areas of human multiple sclerosis lesions, as well as our studies in $MOG_{35–55}$-induced EAE in mice, a classic model of multiple sclerosis. VEGFA and TYMP are both induced specifically in astrocytes in EAE spinal cord lesions, and correlate strongly with other features of the blood–brain barrier breakdown cascade. Moreover, our functional data show that blockade of TYMP signalling significantly reduces clinical severity and tissue pathology in the EAE model, similar to the outcomes seen in mice receiving the inhibitor of VEGFA signalling, cavtratin. Moreover, while inhibition of both TYMP and VEGFA signalling does not produce additional benefits in terms of mean or peak clinical score, which is already reduced substantially by either alone, co-treatment does produce an additional improvement in blood–brain barrier integrity, and this is further associated with enhanced myelin and axon preservation. The lack of a combined effect on clinical disease is interesting, particularly given that the cavtratin concentration used produces a phenotype resembling astrocyte-specific VEGFA inactivation (*mGfapCre:Vegfa*$^{fl/fl}$) (Argaw *et al.*, 2012), and hence indicative of highly efficient VEGFA signalling blockade. It may be that abrogation of blood–brain barrier breakdown has a maximum potential impact on clinical disability in the acute stages of autoimmune demyelination. However, the additional improvement seen in response to co-treatment, in terms of blood–brain barrier integrity and neural preservation, may have consequences for the chronic stages of disease; thus blocking both pathways may hold promise as an approach to maximizing tissue protection.

The discovery of two classic tumour angiogenesis signalling pathways in reactive astrocytosis and inflammatory blood–brain barrier breakdown leads one to speculate as to whether other functionally similar pathways in tumour angiogenesis, such as FGF2 signalling, also play a contributing role in CNS barrier disruption. Given the heterogeneity with which different tumour subtypes employ these various factors, it is also possible that different astrocytic populations may use distinctive inflammatory pathways in different regions of the CNS. In this way, these local determinants might predispose different regions to be more or less susceptible to injury and blood–brain barrier breakdown. Future work comparing mechanisms underlying blood–brain barrier opening in different areas of the brain, particularly those with high or low susceptibility to inflammatory lesion formation, may represent a fruitful approach toward understanding characteristic neuroanatomical patterns of various autoinflammatory CNS conditions,

including neuromyelitis optica, chronic lymphocytic inflammation with pontine perivascular enhancement responsive to steroids (CLIPPERS), and multiple sclerosis.

Interestingly, a human phenotype of TYMP deletion has been described with the paediatric syndrome, mitochondrial neurogastrointestinal encephalomyopathy (MNGIE). Patients have a loss of function mutation in the intron 8 splice acceptor site leading to loss of exon 8 and lower levels of functional TYMP (Wong, 2012). In addition to mitochondrial deficits, attributed to accumulation of thymidine, patients exhibit T_2 hyperintense white matter lesions (Said *et al.*, 2005). It is unclear whether these represent metabolic lesions, or more provocatively, inflammatory lesions secondary to dysregulated blood–brain barrier opening, although the mechanism by which loss of TYMP might lead to white matter lesion formation is unclear. Hypothetically, a homeostatic interaction with the VEGFA pathway or other inflammatory modulators could lead to compensatory activation of pro-permeability pathways.

In summary, the current study suggests roles for two classic tumour angiogenesis pathways in blood–brain barrier breakdown and inflammatory CNS lesion formation. Our data identify astrocytic TYMP as an important astrocyte-derived permeability factor in inflammatory CNS disease, and suggest that it interacts with VEGFA to promote blood–brain barrier breakdown.

Funding

This work was supported by NINDS Research Grants R01NS056074, R01NS062703 and R01NS085103 (G.R.J.), and by NIH R24CA095823 (to the MSSM Microscopy Facility). B.M.L. is the recipient of NIH NRSA predoctoral fellowship F30NS090718. S.H. is the recipient of research residency training grant funding from NIH R25NS079102. Additional support was provided by National MS Society research grants RG4127 and RG5024 (G.R.J.). L.A. is the recipient of National multiple sclerosis Society postdoctoral fellowship FG2005. This work was also supported by the Beker Foundation (G.R.J.), Noto Foundation (G.R.J.), and the Guthy-Jackson Charitable Foundation (G.R.J.).

Supplementary material

Supplementary material is available at *Brain* online.

References

Abdelsaid MA, Matragoon S, El-Remessy AB. Thioredoxin-interacting protein expression is required for VEGF-mediated angiogenic signal in endothelial cells. Antioxid Redox Signal 2013; 19: 2199–212.

Abe K, Takeichi M. EPLIN mediates linkage of the cadherin catenin complex to F-actin and stabilizes the circumferential actin belt. Proc Natl Acad Sci USA 2008; 105: 13–9.

Absinta M, Sati P, Gaitan MI, Maggi P, Cortese IC, Filippi M, et al. Seven-tesla phase imaging of acute multiple sclerosis lesions: a new window into the inflammatory process. Ann Neurol 2013; 74: 669–78.

Adams RA, Bauer J, Flick MJ, Sikorski SL, Nuriel T, Lassmann H, et al. The fibrin-derived gamma377-395 peptide inhibits microglia activation and suppresses relapsing paralysis in central nervous system autoimmune disease. J Exp Med 2007; 204: 571–82.

Agrawal S, Anderson P, Durbeej M, van Rooijen N, Ivars F, Opdenakker G, et al. Dystroglycan is selectively cleaved at the parenchymal basement membrane at sites of leukocyte extravasation in experimental autoimmune encephalomyelitis. J Exp Med 2006; 203: 1007–19.

Alvarez JI, Dodelet-Devillers A, Kebir H, Ifergan I, Fabre PJ, Terouz S, et al. The Hedgehog pathway promotes blood-brain barrier integrity and CNS immune quiescence. Science 2011; 334: 1727–31.

Argaw AT, Asp L, Zhang J, Navrazhina K, Pham T, Mariani JN, et al. Astrocyte-derived VEGFA drives blood-brain barrier disruption in CNS inflammatory disease. J Clin Invest 2012; 122: 2454–68.

Argaw AT, Gurfein BT, Zhang Y, Zameer A, John GR. VEGF-mediated disruption of endothelial CLN-5 promotes blood-brain barrier breakdown. Proc Natl Acad Sci USA 2009; 106: 1977–82.

Argaw AT, Zhang Y, Snyder BJ, Zhao ML, Kopp N, Lee SC, et al. IL-1beta regulates blood-brain barrier permeability via reactivation of the hypoxia-angiogenesis program. J Immunol 2006; 177: 5574–84.

Armulik A, Genove G, Mae M, Nisancioglu MH, Wallgard E, Niaudet C, et al. Pericytes regulate the blood-brain barrier. Nature 2010; 468: 557–61.

Asada M, Ebihara S, Yamanda S, Niu K, Okazaki T, Sora I, et al. Depletion of serotonin and selective inhibition of 2B receptor suppressed tumor angiogenesis by inhibiting endothelial nitric oxide synthase and extracellular signal-regulated kinase 1/2 phosphorylation. Neoplasia 2009; 11: 408–17.

Badea T, Niculescu F, Soane L, Fosbrink M, Sorana H, Rus V, et al. RGC-32 increases p34CDC2 kinase activity and entry of aortic smooth muscle cells into S-phase. J Biol Chem 2002; 277: 502–8.

Bar-Or A, Nuttall RK, Duddy M, Alter A, Kim HJ, Ifergan I, et al. Analyses of all matrix metalloproteinase members in leukocytes emphasize monocytes as major inflammatory mediators in multiple sclerosis. Brain 2003; 126(Pt 12): 2738–49.

Bell RD, Winkler EA, Sagare AP, Singh I, LaRue B, Deane R, et al. Pericytes control key neurovascular functions and neuronal phenotype in the adult brain and during brain aging. Neuron 2010; 68: 409–27.

Bijnsdorp IV, Capriotti F, Kruyt FA, Losekoot N, Fukushima M, Griffioen AW, et al. Thymidine phosphorylase in cancer cells stimulates human endothelial cell migration and invasion by the secretion of angiogenic factors. Br J Cancer 2011; 104: 1185–92.

Bogler O, Noble M. Measurement of time in oligodendrocyte-type-2 astrocyte (O-2A) progenitors is a cellular process distinct from differentiation or division. Dev Biol 1994; 162: 525–38.

Brosnan CF, Cannella B, Battistini L, Raine CS. Cytokine localization in multiple sclerosis lesions: correlation with adhesion molecule expression and reactive nitrogen species. Neurology 1995; 45 (6 Suppl 6): S16–21.

Bruck W, Bitsch A, Kolenda H, Bruck Y, Stiefel M, Lassmann H. Inflammatory central nervous system demyelination: correlation of magnetic resonance imaging findings with lesion pathology. Ann Neurol 1997; 42: 783–93.

Bush TG, Puvanachandra N, Horner CH, Polito A, Ostenfeld T, Svendsen CN, et al. Leukocyte infiltration, neuronal degeneration, and neurite outgrowth after ablation of scar-forming, reactive astrocytes in adult transgenic mice. Neuron 1999; 23: 297–308.

Carmeliet P, Ferreira V, Breier G, Pollefeyt S, Kieckens L, Gertsenstein M, et al. Abnormal blood vessel development and lethality in embryos lacking a single VEGF allele. Nature 1996; 380: 435–9.

Caunt M, Hu L, Tang T, Brooks PC, Ibrahim S, Karpatkin S. Growth-regulated oncogene is pivotal in thrombin-induced angiogenesis. Cancer Res 2006; 66: 4125–32.

Collins PD, Connolly DT, Williams TJ. Characterization of the increase in vascular permeability induced by vascular permeability factor *in vivo*. Br J Pharmacol 1993; 109: 195–9.

Cox CM, D'Agostino SL, Miller MK, Heimark RL, Krieg PA. Apelin, the ligand for the endothelial G-protein-coupled receptor, APJ, is a potent angiogenic factor required for normal vascular development of the frog embryo. Dev Biol 2006; 296: 177–89.

Dallasta LM, Pisarov LA, Esplen JE, Werley JV, Moses AV, Nelson JA, et al. Blood-brain barrier tight junction disruption in human immunodeficiency virus-1 encephalitis. Am J Pathol 1999; 155: 1915–27.

Daneman R, Zhou L, Kebede AA, Barres BA. Pericytes are required for blood-brain barrier integrity during embryogenesis. Nature 2010; 468: 562–6.

DeAngelis T, Lublin F. Multiple sclerosis: new treatment trials and emerging therapeutic targets. Curr Opin Neurol 2008; 21: 261–71.

Dobrogowska DH, Lossinsky AS, Tarnawski M, Vorbrodt AW. Increased blood-brain barrier permeability and endothelial abnormalities induced by vascular endothelial growth factor. J Neurocytol 1998; 27: 163–73.

Dulak J, Loboda A, Zagorska A, Jozkowicz A. Complex role of heme oxygenase-1 in angiogenesis. Antioxid Redox Signal 2004; 6: 858–66.

Ellis PE, Wong Te Fong LF, Rolfe KJ, Crow JC, Reid WM, Davidson T, et al. The role of vascular endothelial growth factor-A (VEGFA) and platelet-derived endothelial cell growth factor/thymidine phosphorylase (PD-ECGF/TP) in Paget's disease of the vulva and breast. Anticancer Res 2002; 22: 857–61.

Engelhardt B, Liebner S. Novel insights into the development and maintenance of the blood-brain barrier. Cell Tissue Res 2014; 355: 687–99.

Engels K, Fox SB, Whitehouse RM, Gatter KC, Harris AL. Up-regulation of thymidine phosphorylase expression is associated with a discrete pattern of angiogenesis in ductal carcinomas in situ of the breast. J Pathol 1997; 182: 414–20.

Ferrara N, Carver-Moore K, Chen H, Dowd M, Lu L, O'Shea KS, et al. Heterozygous embryonic lethality induced by targeted inactivation of the VEGF gene. Nature 1996; 380: 439–42.

Flynn KM, Michaud M, Canosa S, Madri JA. CD44 regulates vascular endothelial barrier integrity via a PECAM-1 dependent mechanism. Angiogenesis 2013; 16: 689–705.

Furukawa T, Yoshimura A, Sumizawa T, Haraguchi M, Akiyama S, Fukui K, et al. Angiogenic factor. Nature 1992; 356: 668.

Garcia AD, Doan NB, Imura T, Bush TG, Sofroniew MV. GFAP-expressing progenitors are the principal source of constitutive neurogenesis in adult mouse forebrain. Nat Neurosci 2004; 7: 1233–41.

Gerber HP, Hillan KJ, Ryan AM, Kowalski J, Keller GA, Rangell L, et al. VEGF is required for growth and survival in neonatal mice. Development 1999; 126: 1149–59.

Germano A, Caffo M, Angileri FF, Arcadi F, Newcomb-Fernandez J, Caruso G, et al. NMDA receptor antagonist felbamate reduces behavioral deficits and blood-brain barrier permeability changes after experimental subarachnoid hemorrhage in the rat. J Neurotrauma 2007; 24: 732–44.

Gorina R, Lyck R, Vestweber D, Engelhardt B. beta2 integrin-mediated crawling on endothelial ICAM-1 and ICAM-2 is a prerequisite for transcellular neutrophil diapedesis across the inflamed blood-brain barrier. J Immunol 2014; 192: 324–37.

Graesser D, Solowiej A, Bruckner M, Osterweil E, Juedes A, Davis S, et al. Altered vascular permeability and early onset of experimental autoimmune encephalomyelitis in PECAM-1-deficient mice. J Clin Invest 2002; 109: 383–92.

Gurfein BT, Zhang Y, Lopez CB, Argaw AT, Zameer A, Moran TM, et al. IL-11 regulates autoimmune demyelination. J Immunol 2009; 183: 4229–40.

Harjes U, Bridges E, McIntyre A, Fielding BA, Harris AL. Fatty acid binding protein 4, a point of convergence for angiogenic and metabolic signalling pathways in endothelial cells. J Biol Chem 2014.

Hawkins BT, Davis TP. The blood-brain barrier/neurovascular unit in health and disease. Pharmacol Rev 2005; 57: 173–85.

Hayashi Y, Nomura M, Yamagishi S, Harada S, Yamashita J, Yamamoto H. Induction of various blood-brain barrier properties in non-neural endothelial cells by close apposition to co-cultured astrocytes. Glia 1997; 19: 13–26.

Herx LM, Yong VW. Interleukin-1 beta is required for the early evolution of reactive astrogliosis following CNS lesion. J Neuropathol Exp Neurol 2001; 60: 961–71.

Hosokawa T, Nakajima H, Doi Y, Sugino M, Kimura F, Hanafusa T, et al. Increased serum matrix metalloproteinase-9 in neuromyelitis optica: implication of disruption of blood-brain barrier. J Neuroimmunol 2011; 236: 81–6.

Hotchkiss KA, Basile CM, Spring SC, Bonuccelli G, Lisanti MP, Terman BI. TEM8 expression stimulates endothelial cell adhesion and migration by regulating cell-matrix interactions on collagen. Exp Cell Res 2005; 305: 133–44.

Huang S, Bucana CD, Van Arsdall M, Fidler IJ. Stat1 negatively regulates angiogenesis, tumorigenicity and metastasis of tumor cells. Oncogene 2002; 21: 2504–12.

Hudson N, Powner MB, Sarker MH, Burgoyne T, Campbell M, Ockrim ZK, et al. Differential apicobasal VEGF signaling at vascular blood-neural barriers. Dev Cell 2014; 30: 541–52.

Hurwitz AA, Lyman WD, Guida MP, Calderon TM, Berman JW. Tumor necrosis factor alpha induces adhesion molecule expression on human fetal astrocytes. J Exp Med 1992; 176: 1631–6.

Igarashi M, Dhar DK, Kubota H, Yamamoto A, El-Assal O, Nagasue N. The prognostic significance of microvessel density and thymidine phosphorylase expression in squamous cell carcinoma of the esophagus. Cancer 1998; 82: 1225–32.

Ishikawa F, Miyazono K, Hellman U, Drexler H, Wernstedt C, Hagiwara K, et al. Identification of angiogenic activity and the cloning and expression of platelet-derived endothelial cell growth factor. Nature 1989; 338: 557–62.

Jeltsch M, Kaipainen A, Joukov V, Meng X, Lakso M, Rauvala H, et al. Hyperplasia of lymphatic vessels in VEGF-C transgenic mice. Science 1997; 276: 1423–5.

John GR, Chen L, Rivieccio MA, Melendez-Vasquez CV, Hartley A, Brosnan CF. Interleukin-1beta induces a reactive astroglial phenotype via deactivation of the Rho GTPase-Rock axis. J Neurosci 2004; 24: 2837–45.

John GR, Simpson JE, Woodroofe MN, Lee SC, Brosnan CF. Extracellular nucleotides differentially regulate interleukin-1beta signaling in primary human astrocytes: implications for inflammatory gene expression. J Neurosci 2001; 21: 4134–42.

Ju R, Cirone P, Lin S, Griesbach H, Slusarski DC, Crews CM. Activation of the planar cell polarity formin DAAM1 leads to inhibition of endothelial cell proliferation, migration, and angiogenesis. Proc Natl Acad Sci USA 2010; 107: 6906–11.

Kim MO, Suh HS, Brosnan CF, Lee SC. Regulation of RANTES/CCL5 expression in human astrocytes by interleukin-1 and interferon-beta. J Neurochem 2004; 90: 297–308.

Kirk S, Frank JA, Karlik S. Angiogenesis in multiple sclerosis: is it good, bad or an epiphenomenon? J Neurol Sci 2004; 217: 125–30.

Kletsas D, Barbieri D, Stathakos D, Botti B, Bergamini S, Tomasi A, et al. The highly reducing sugar 2-deoxy-D-ribose induces apoptosis in human fibroblasts by reduced glutathione depletion and cytoskeletal disruption. Biochem Biophys Res Commun 1998; 243: 416–25.

Koukourakis MI, Giatromanolaki A, O'Byrne KJ, Comley M, Whitehouse RM, Talbot DC, et al. Platelet-derived endothelial cell growth factor expression correlates with tumour angiogenesis and prognosis in non-small-cell lung cancer. Br J Cancer 1997; 75: 477–81.

Kunitomi A, Hori T, Imura A, Uchiyama T. Vascular endothelial cells provide T cells with costimulatory signals via the OX40/gp34 system. J Leukoc Biol 2000; 68: 111–8.

Larrucea S, Butta N, Arias-Salgado EG, Alonso-Martin S, Ayuso MS, Parrilla R. Expression of podocalyxin enhances the adherence, migration, and intercellular communication of cells. Exp Cell Res 2008; 314: 2004–15.

Lee SC, Liu W, Brosnan CF, Dickson DW. Characterization of primary human fetal dissociated central nervous system cultures with an emphasis on microglia. Lab Invest 1992; 67: 465–76.

Lee SW, Kim WJ, Choi YK, Song HS, Son MJ, Gelman IH, et al. SSeCKS regulates angiogenesis and tight junction formation in blood-brain barrier. Nat Med 2003; 9: 900–6.

Leung DW, Cachianes G, Kuang WJ, Goeddel DV, Ferrara N. Vascular endothelial growth factor is a secreted angiogenic mitogen. Science 1989; 246: 1306–9.

Li L, Welser JV, Dore-Duffy P, del Zoppo GJ, Lamanna JC, Milner R. In the hypoxic central nervous system, endothelial cell proliferation is followed by astrocyte activation, proliferation, and increased expression of the alpha 6 beta 4 integrin and dystroglycan. Glia 2010; 58: 1157–67.

Ludwin SK. HJM, McFarland H.F. Vascular proliferation and angiogenesis in multiple sclerosis: clinical and pathogenetic implications. J Neuropathol Exp Neurol 2001; 60: 505.

Lyck R, Engelhardt B. Going against the tide–how encephalitogenic T cells breach the blood-brain barrier. J Vasc Res 2012; 49: 497–509.

Maeda K, Chung YS, Ogawa Y, Takatsuka S, Kang SM, Ogawa M, et al. Thymidine phosphorylase/platelet-derived endothelial cell growth factor expression associated with hepatic metastasis in gastric carcinoma. Br J Cancer 1996; 73: 884–8.

Miller DH, Grossman RI, Reingold SC, McFarland HF. The role of magnetic resonance techniques in understanding and managing multiple sclerosis. Brain 1998; 121 (Pt 1): 3–24.

Moghaddam A, Zhang HT, Fan TP, Hu DE, Lees VC, Turley H, et al. Thymidine phosphorylase is angiogenic and promotes tumor growth. Proc Natl Acad Sci USA 1995; 92: 998–1002.

Muramatsu R, Takahashi C, Miyake S, Fujimura H, Mochizuki H, Yamashita T. Angiogenesis induced by CNS inflammation promotes neuronal remodeling through vessel-derived prostacyclin. Nat Med 2012; 18: 1658–64.

Nag S, Papneja T, Venugopalan R, Stewart DJ. Increased angiopoietin2 expression is associated with endothelial apoptosis and blood-brain barrier breakdown. Lab Invest 2005; 85: 1189–98.

Nielsen JS, McNagny KM. Novel functions of the CD34 family. J Cell Sci 2008; 121(Pt 22): 3683–92.

Nitta T, Hata M, Gotoh S, Seo Y, Sasaki H, Hashimoto N, et al. Size-selective loosening of the blood-brain barrier in claudin-5-deficient mice. J Cell Biol 2003; 161: 653–60.

Nolz JC, Harty JT. IL-15 regulates memory CD8+ T cell O-glycan synthesis and affects trafficking. J Clin Invest 2014; 124: 1013–26.

Olsson AK, Dimberg A, Kreuger J, Claesson-Welsh L. VEGF receptor signalling - in control of vascular function. Nat Rev Mol Cell Biol 2006; 7: 359–71.

Park SY, Shi X, Pang J, Yan C, Berk BC. Thioredoxin-interacting protein mediates sustained VEGFR2 signaling in endothelial cells required for angiogenesis. Arterioscler Thromb Vasc Biol 2013; 33: 737–43.

Peiffer I, Belhomme D, Barbet R, Haydont V, Zhou YP, Fortunel NO, et al. Simultaneous differentiation of endothelial and trophoblastic cells derived from human embryonic stem cells. Stem Cells Dev 2007; 16: 393–402.

Proescholdt MA, Jacobson S, Tresser N, Oldfield EH, Merrill MJ. Vascular endothelial growth factor is expressed in multiple sclerosis plaques and can induce inflammatory lesions in experimental allergic encephalomyelitis rats. J Neuropathol Exp Neurol 2002; 61: 914–25.

Ransohoff RM, Glabinski A, Tani M. Chemokines in immune-mediated inflammation of the central nervous system. Cytokine Growth Factor Rev 1996; 7: 35–46.

Roudnicky F, Poyet C, Wild P, Krampitz S, Negrini F, Huggenberger R, et al. Endocan is upregulated on tumor vessels in invasive bladder cancer where it mediates VEGFA-induced angiogenesis. Cancer Res 2013; 73: 1097–106.

Saeki T, Tanada M, Takashima S, Saeki H, Takiyama W, Nishimoto N, et al. Correlation between expression of platelet-derived endothelial cell growth factor (thymidine phosphorylase) and microvessel density in early-stage human colon carcinomas. Jpn J Clin Oncol 1997; 27: 227–30.

Said G, Lacroix C, Plante-Bordeneuve V, Messing B, Slama A, Crenn P, et al. Clinicopathological aspects of the neuropathy of neurogastrointestinal encephalomyopathy (MNGIE) in four patients including two with a Charcot-Marie-Tooth presentation. J Neurol 2005; 252: 655–62.

Saitou M, Fujimoto K, Doi Y, Itoh M, Fujimoto T, Furuse M, et al. Occludin-deficient embryonic stem cells can differentiate into polarized epithelial cells bearing tight junctions. J Cell Biol 1998; 141: 397–408.

Sandoval KE, Witt KA. Blood-brain barrier tight junction permeability and ischemic stroke. Neurobiol Dis 2008; 32: 200–19.

Sato Y, Teruyama K, Nakano T, Oda N, Abe M, Tanaka K, et al. Role of transcription factors in angiogenesis: Ets-1 promotes angiogenesis as well as endothelial apoptosis. Ann N Y Acad Sci 2001; 947: 117–23.

Schachtrup C, Lu P, Jones LL, Lee JK, Lu J, Sachs BD, et al. Fibrinogen inhibits neurite outgrowth via beta 3 integrin-mediated phosphorylation of the EGF receptor. Proc Natl Acad Sci USA 2007; 104: 11814–9.

Schluesener HJ, Sobel RA, Linington C, Weiner HL. A monoclonal antibody against a myelin oligodendrocyte glycoprotein induces relapses and demyelination in central nervous system autoimmune disease. J Immunol 1987; 139: 4016–21.

Shimizu F, Sano Y, Takahashi T, Haruki H, Saito K, Koga M, et al. Sera from neuromyelitis optica patients disrupt the blood-brain barrier. J Neurol Neurosurg Psychiatry 2012; 83: 288–97.

Sjostrom M, Jakobsson PJ, Heimburger M, Palmblad J, Haeggstrom JZ. Human umbilical vein endothelial cells generate leukotriene C4 via microsomal glutathione S-transferase type 2 and express the CysLT(1) receptor. Eur J Biochem 2001; 268: 2578–86.

Soker S, Takashima S, Miao HQ, Neufeld G, Klagsbrun M. Neuropilin-1 is expressed by endothelial and tumor cells as an isoform-specific receptor for vascular endothelial growth factor. Cell 1998; 92: 735–45.

Takanami I, Tanaka F, Hashizume T, Kodaira S. Vascular endothelial growth factor and its receptor correlate with angiogenesis and survival in pulmonary adenocarcinoma. Anticancer Res 1997; 17: 2811–4.

Takao S, Takebayashi Y, Che X, Shinchi H, Natsugoe S, Miyadera K, et al. Expression of thymidine phosphorylase is associated with a poor prognosis in patients with ductal adenocarcinoma of the pancreas. Clin Cancer Res 1998; 4: 1619–24.

Tanaka A, Itoh F, Nishiyama K, Takezawa T, Kurihara H, Itoh S, et al. Inhibition of endothelial cell activation by bHLH protein E2-2 and its impairment of angiogenesis. Blood 2010; 115: 4138–47.

Tang X, Jin R, Qu G, Wang X, Li Z, Yuan Z, et al. GPR116, an adhesion G-protein-coupled receptor, promotes breast cancer metastasis via the Galphaq-p63RhoGEF-Rho GTPase pathway. Cancer Res 2013; 73: 6206–18.

Tang Y, Pacary E, Freret T, Divoux D, Petit E, Schumann-Bard P, et al. Effect of hypoxic preconditioning on brain genomic response

before and following ischemia in the adult mouse: identification of potential neuroprotective candidates for stroke. Neurobiol Dis 2006; 21: 18–28.

Toi M, Inada K, Hoshina S, Suzuki H, Kondo S, Tominaga T. Vascular endothelial growth factor and platelet-derived endothelial cell growth factor are frequently coexpressed in highly vascularized human breast cancer. Clin Cancer Res 1995; 1: 961–4.

Tsujitani S, Saito H, Maeta Y, Yamaguchi K, Tatebe S, Kondo A, et al. Neoangiogenesis in patients with gastric carcinoma in relation to the expression of vascular endothelial growth factor and thymidine phosphorylase. Anticancer Res 2004; 24: 1853–9.

Uchida S, Shimada Y, Watanabe G, Tanaka H, Shibagaki I, Miyahara T, et al. In oesophageal squamous cell carcinoma vascular endothelial growth factor is associated with p53 mutation, advanced stage and poor prognosis. Br J Cancer 1998; 77: 1704–9.

Vallabhapurapu S, Karin M. Regulation and function of NF-kappaB transcription factors in the immune system. Annu Rev Immunol 2009; 27: 693–733.

Vazquez F, Hastings G, Ortega MA, Lane TF, Oikemus S, Lombardo M, et al. METH-1, a human ortholog of ADAMTS-1, and METH-2 are members of a new family of proteins with angio-inhibitory activity. J Biol Chem 1999; 274: 23349–57.

Warton K, Foster NC, Gold WA, Stanley KK. A novel gene family induced by acute inflammation in endothelial cells. Gene 2004; 342: 85–95.

Wenke AK, Rothhammer T, Moser M, Bosserhoff AK. Regulation of integrin alpha10 expression in chondrocytes by the transcription factors AP-2epsilon and Ets-1. Biochem Biophys Res Commun 2006; 345: 495–501.

Wolburg H, Wolburg-Buchholz K, Kraus J, Rascher-Eggstein G, Liebner S, Hamm S, et al. Localization of claudin-3 in tight junctions of the blood-brain barrier is selectively lost during experimental autoimmune encephalomyelitis and human glioblastoma multiforme. Acta Neuropathol 2003; 105: 586–92.

Wong LJ. Mitochondrial syndromes with leukoencephalopathies. Semin Neurol 2012; 32: 55–61.

Yeo KT, Wang HH, Nagy JA, Sioussat TM, Ledbetter SR, Hoogewerf AJ, et al. Vascular permeability factor (vascular endothelial growth factor) in guinea pig and human tumor and inflammatory effusions. Cancer Res 1993; 53: 2912–8.

Yin KJ, Hamblin M, Chen YE. Non-coding RNAs in cerebral endothelial pathophysiology: Emerging roles in stroke. Neurochem Int 2014; 77: 9–16.

Zhang Y, Taveggia C, Melendez-Vasquez C, Einheber S, Raine CS, Salzer JL, et al. Interleukin-11 potentiates oligodendrocyte survival and maturation, and myelin formation. J Neurosci 2006; 26: 12174–85.

Zlokovic BV. The blood-brain barrier in health and chronic neurodegenerative disorders. Neuron 2008; 57: 178–201.